LITHOS 452-453 (2023) 107206

Contents lists available at ScienceDirect

LITHOS

journal homepage: www.elsevier.com/locate/lithos

Geochemistry of 2.45 Ga mafic dykes in northern Finland: Constraints on the petrogenesis and PGE prospectivity of coeval layered intrusions

Fang-Fang Guo [a,*], Wolfgang D. Maier [b], Jussi S. Heinonen [c], Eero Hanski [a], Jouni Vuollo [d], Sarah-Jane Barnes [e], Yann Lahaye [f], Hannu Huhma [f], Shenghong Yang [a]

[a] Oulu Mining School, Faculty of Technology, University of Oulu, Oulu 90014, Finland
[b] School of Earth and Environmental Sciences, Cardiff University, Cardiff CF10 3AT, Wales, UK
[c] Department of Geosciences and Geography, University of Helsinki, Helsinki 00014, Finland
[d] Geological Survey of Finland, Rovaniemi 96100, Finland
[e] Science de la Terre, Université du Québec à Chicoutimi, Chicoutimi, QC G7H 2B1, Canada
[f] Geological Survey of Finland, Espoo 02150, Finland

ARTICLE INFO

Keywords:
Platinum-group elements
Mafic dykes
Sr isotopes
Thermal dynamic modelling
Palaeoproterozoic
Northern Finland

ABSTRACT

The Karelian craton contains abundant ~2.45 Ga mafic dykes that are compositionally, temporally and, in some cases, spatially related to PGE-mineralised mafic-ultramafic layered intrusions. The dykes can be sub-divided into four groups, namely siliceous high-magnesian basalts (SHMB), gabbronorites (GBNO), low-Ti tholeiites and Fe-rich tholeiites. In this study, we group the SHMB and GBNO dykes to one group as SHMB group, and the two tholeiitic group dykes as tholeiite group, based on their similar geochemical and mineralogical features. In the SHMB group dykes, plagioclase has initial $^{87}Sr/^{86}Sr$ ratios of 0.7028 to 0.7036 and initial bulk-rock εNd values vary from −2.5 to −1.0, indicating moderate degrees of contamination with Archaean basement. Tholeiitic dykes show a less-radiogenic Sr isotope composition with an average initial $^{87}Sr/^{86}Sr$ ratio of 0.7024 and higher initial εNd values ranging from +0.3 to +1.7. Thermodynamic and geochemical modelling suggests that the SHMB group dykes could have formed by crustal contamination of a komatiitic magma at deeper crust followed by fractional crystallisation at shallower depth, whereas the tholeiitic group mainly experienced fractional crystallisation with less crustal contamination. Alternatively, the SHMB dykes may have been derived from a SCLM mantle whereas tholeiitic dykes from a plume mantle, or the two types of dykes derived from different part of a mantle plume with different melting degrees, though these latter two models are not favoured in this study. Based on trace element and isotope characteristics, the SHMB dykes are suitable candidates for the parental magmas to some of the Finnish PGE-mineralised intrusions (e.g., Penikat and Portimo), whereas the tholeiitic dykes may represent the parental magma of the Tsipringa layered intrusion in Russia. Both the SHMB and tholeiitic dyke types are fertile with regard to PGE, with up to 10–20 ppb Pt and Pd and mantle-like Cu/Pd ratios in their least evolved members, suggesting that the magmas remained sulphide undersaturated during mantle melting and *en route* to the upper crust. This interpretation is consistent with the fact that most of the ~2.45 Ga Fennoscandian layered intrusions contain PGE mineralisation. Sulphide melt saturation in the dykes and layered intrusions was mostly attained after their final emplacement, likely due to crystal fractionation.

1. Introduction

Mafic layered intrusions are host to significant mineral resources, particularly Cr, PGE, Ti and V, as well as Ni, Cu, Co and Au as by-products (Smith and Maier, 2021). Many of these metals (except Au, Cr) are defined as critical raw materials and/or green transition raw materials (e.g., European Commission, 2020). To develop sustainable exploration methods with lower environmental and social impact, efficient regional-scale exploration targeting is crucial. This requires accurate and highly refined ore models, but for most layered intrusions, one of the main obstacles is the insufficient knowledge of the composition of the parental magmas. The intrusions consist largely of slowly cooled, highly equilibrated cumulate rocks though some have chilled margins that can potentially provide clues to the parental magma composition.

* Corresponding author.
E-mail address: fangfang.guo@oulu.fi (F.-F. Guo).

https://doi.org/10.1016/j.lithos.2023.107206
Received 8 September 2022; Received in revised form 3 May 2023; Accepted 3 May 2023
Available online 15 May 2023

However, in many cases, the exposed chilled rocks may not represent the most primitive magma, as primary chilled margins could be remelted by the constant heat flux from the magma, or they may be contaminated by local-scale interaction with immediate country rocks (Huppert and Sparks, 1989; Maier et al., 2018). Therefore, many previous workers have attempted to constrain the parental magma composition by studying spatially or temporally associated mafic sills and dykes (Barnes et al., 2010; Helz, 1995; Wang et al., 2011). In the case of the Karelian and Kola cratons, this approach is particularly promising because a number of mafic layered intrusions with ages of ~2.45 Ga host significant mineralisation, and they are spatially and temporally associated with abundant mafic dykes, which likely belong to the same magmatic event (Iljina et al., 2015; Maier et al., 2018; Maier and Hanski, 2017; Vuollo and Huhma, 2005).

In the present study, we provide new compositional data for 37 dykes from the Karelian craton, including mineral chemistry, bulk-rock major element, lithophile trace element and PGE compositions, as well as in-situ Sr isotope compositions of plagioclase. We also present results of thermodynamic modelling and draw comparisons with mafic-ultramafic magmatism across the Fennoscandian Shield and globally, to constrain the petrogenesis of the dykes and evaluate the ore formation potential of correlated layered intrusions.

2. Geological background

Archaean rocks are widely distributed in the NE Fennoscandia in different cratons (Kola, Karelian, Belamorian and Norrbotten), that are mainly composed of greenstone belts and different types of granitoids (Hölttä et al., 2012). Several Mesoarchean microcratons accreted together in the Neoarchaean, forming the Kenorland supercontinent. In Finland, the Karelia craton is divided into four major blocks: Kuhmo, Taivalkoski, Pudasjärvi, and Iisalmi (Hölttä et al., 2012; Vuollo and Huhma, 2005) (Fig. 1). Across much of the NE Fennoscandian Shield, including the Karelian craton and the adjacent Belomorian and Kola cratons, widespread mafic-ultramafic magmatism occurred at ~2.5–2.45 Ga (Vuollo and Huhma, 2005). It has been suggested that this magmatism has a genetic link to the coeval magmatism in the Superior craton, Canada, representing one of the oldest known large igneous provinces (LIP) on Earth, which initiated the breakup of the Archaean Kenorland supercontinent (Ernst and Bleeker, 2010; Vogel et al., 1998).

The ~2.45–2.5 Ga Fennoscandian magmatism is composed of numerous mafic layered intrusions, mafic dyke swarms, mafic-

Fig. 1. Geological map showing the distribution of 2.45 Ga mafic dykes swarms in the Karelian Craton. Modified after Vuollo and Huhma (2005). Detailed geology map of two layered intrusions Penikat and Portimo complex are shown in Fig. 2. Age data are from Vuollo and Huhma, 2005 and Huhma et al., 2018.

ultramafic volcanic rocks, and minor felsic intrusive and volcanic rocks (Hanski et al., 2001; Huhma et al., 2018; Maier et al., 2018; Puchtel et al., 1998). The 2.5 Ga magmatism is restricted to the Kola Penisula, including the Mochegorsk, Fedorovo-Pansky and Mt. Generalskaya intrusions and the Olenogorsk dyke, while the ~2.45 Ga igneous rocks occur both in the Kola (e.g. Imandra) and the Karelian cratons. The Karelian craton contains Kemi, Penikat, Portimo, Koillismaa, Näränkavaara, Lukkulaisvaara, Tsipringa, and Kivakka intrusions or intrusion complexes in the Tornio–Näränkävaara intrusive belt across Finland and its continuation in Russia, and Koitelainen and Akanvaara intrusions in Finnish Lapland (Amelin et al., 1995; Bayanova et al., 2019; Hanski et al., 2001). Several of the 2.5–2.45 Ga mafic layered intrusions in the Fennoscandian Shield host significant mineralisation of PGE-(Ni-Cu-Co) (e.g., Penikat, Portimo, Koillismaa, Fedorova Pansky, Monchegorsk), chromium (e.g., Kemi, Monchegorsk, Koitelainen, Akanvaara), and vanadium (e.g., Koitelainen, Koillismaa, Akanvaara) (Alapieti et al., 1990; Halkoaho et al., 1990; Hanski et al., 2001; Hanski, 2012; Karinen, 2010; Karinen et al., 2015, Karinen et al., 2022; Karykowski et al., 2018; Maier et al., 2018; Mokrushin et al., 2021; Mutanen, 1997; Schissel et al., 2002;). At present, only one deposit (Kemi, Cr) is under production (Huhtelin, 2015), but mining has occurred previously at Koillismaa (for V) and Monchegorsk (Cr, PGE, Cu—Ni), and many exploration projects are under development (Huhtelin, 2015; Karinen et al., 2015) (Fig. 1).

The ~2.45 Ga dyke swarms, which form the focus of this study, are present in all the blocks of the Karelian craton with the exception of the Iisalmi block. Based on their geochemistry and mineralogy, Vuollo and Huhma (2005) subdivided these dykes into five major groups: 1) boninites, 2) gabbronorites GBNO), 3) low-Ti tholeiites (LTTH), 4) Fe-tholeiites (FTH), and 5) orthopyroxene-plagioclase-phyric dykes, with the latest type being restricted to a few localities in the Kuhmo block. Since boninite is a term that is mainly applied to high-Mg, low-Ti volcanic rocks in fore-arc settings (Hickey and Frey, 1982), we replace it with the term siliceous high-magnesium basalt (SHMB) in this study.

The SHMB dykes are mainly NE–SW-trending and found throughout the Karelian block. Some of them are spatially associated with the 2.45 Ga layered intrusions of the Tornio–Näränkävaara belt and related intrusions in Russian (Iljina et al., 2015). In the Suhanko area (Fig. 2a), some dykes are oriented subparallel to the basal contact of the small Konttijärvi layered intrusion (Iljina et al., 1992) (Fig. 2a), whereas further to the west, on the SE side of the Penikat layered intrusion, the Loljunmaa dyke trends approximately perpendicular to the strike of the intrusion and is interpreted to be its feeder conduit (Maier et al., 2018) (Fig. 2b). The SHMB dykes are 20–60 m thick, and some of them can be traced along strike for >40 km (Vuollo and Huhma, 2005). The rocks are mainly medium grained and consist of plagioclase (35 vol%), orthopyroxene (30 vol%), clinopyroxene (20 vol%), with small amounts of olivine (5 vol%, found in two samples only), chromite and Fe—Ti oxides (Fig. 3a). The dykes show internal variation in grain size, with the margins being relatively fine-grained (Vuollo and Huhma, 2005).

The GBNO dykes are typically NW–SE-trending (~310°). Their thickness reaches 50 m, and they can be followed for a few kilometres along strike. A precise baddeleyite U—Pb age of 2447 ± 10 Ma has been obtained for a dyke in the Suoperä area, ~10 km east of the Russian–Finnish border (Huhma et al., 2018). The dykes are fine grained at their margins but are medium grained in their central parts (Figs. 3c, d). The GBNO dykes are richer in plagioclase (~60 vol%) than the SHMB dykes and have broadly similar clinopyroxene contents (25 vol%), but lower contents of orthopyroxene (5–10 vol%) and olivine (1–2 vol%). Biotite and Fe-Ti-oxides are minor or accessory phases (Figs. 3c, d).

The LTTH dykes occur in the Kuhmo and Pudasjärvi blocks (Vuollo and Huhma, 2005). The width of the dykes is up to tens of metres, and they extend for up to ~2 km along strike. The rocks generally show ophitic textures and are mainly composed of plagioclase (50 vol%), clinopyroxene (35 vol%), and minor amounts of orthopyroxene (2 vol %), quartz, secondary amphibole and Fe-Ti-V oxides (Figs. 3e, f).

The FTH dykes are mainly composed of plagioclase (60 vol%) and clinopyroxene (30 vol%). The main difference between the LTTH and FTH dykes is that the latter have a significant amount of Fe-Ti-oxides (5–10 vol%). Quartz and biotite are of minor abundance (Fig. 3). Only one 10-m-wide dyke in the Taivalkoski area has been dated, yielding a Sm—Nd isochron age of 2407 ± 35 Ma with an initial εNd value of +1.6 (Vuollo and Huhma, 2005) (Figs. 3g, h).

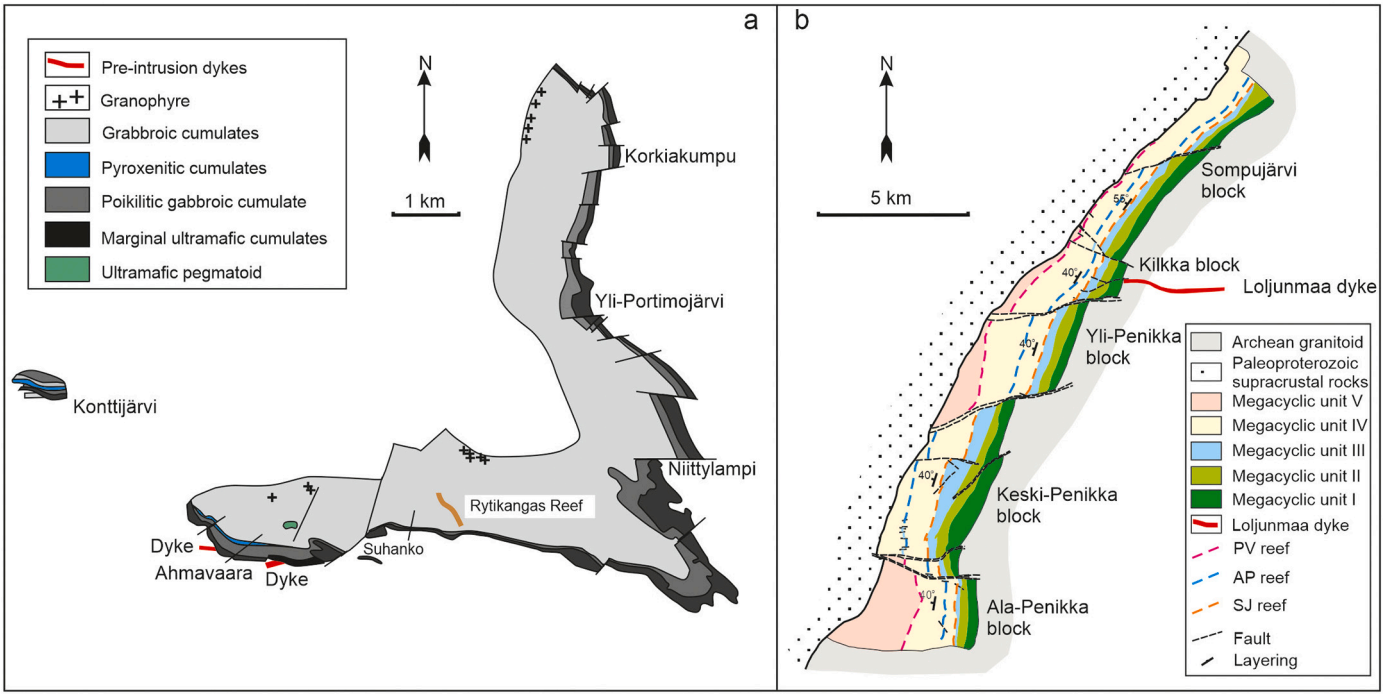

Fig. 2. A. Spatial correlation between mafic dykes and the Suhanko layered intrusion (modified after Iljina et al., 1992); B. Spatial correlation between the Loljunmaa dyke and the Penikat intrusion (modified after Maier et al., 2018).

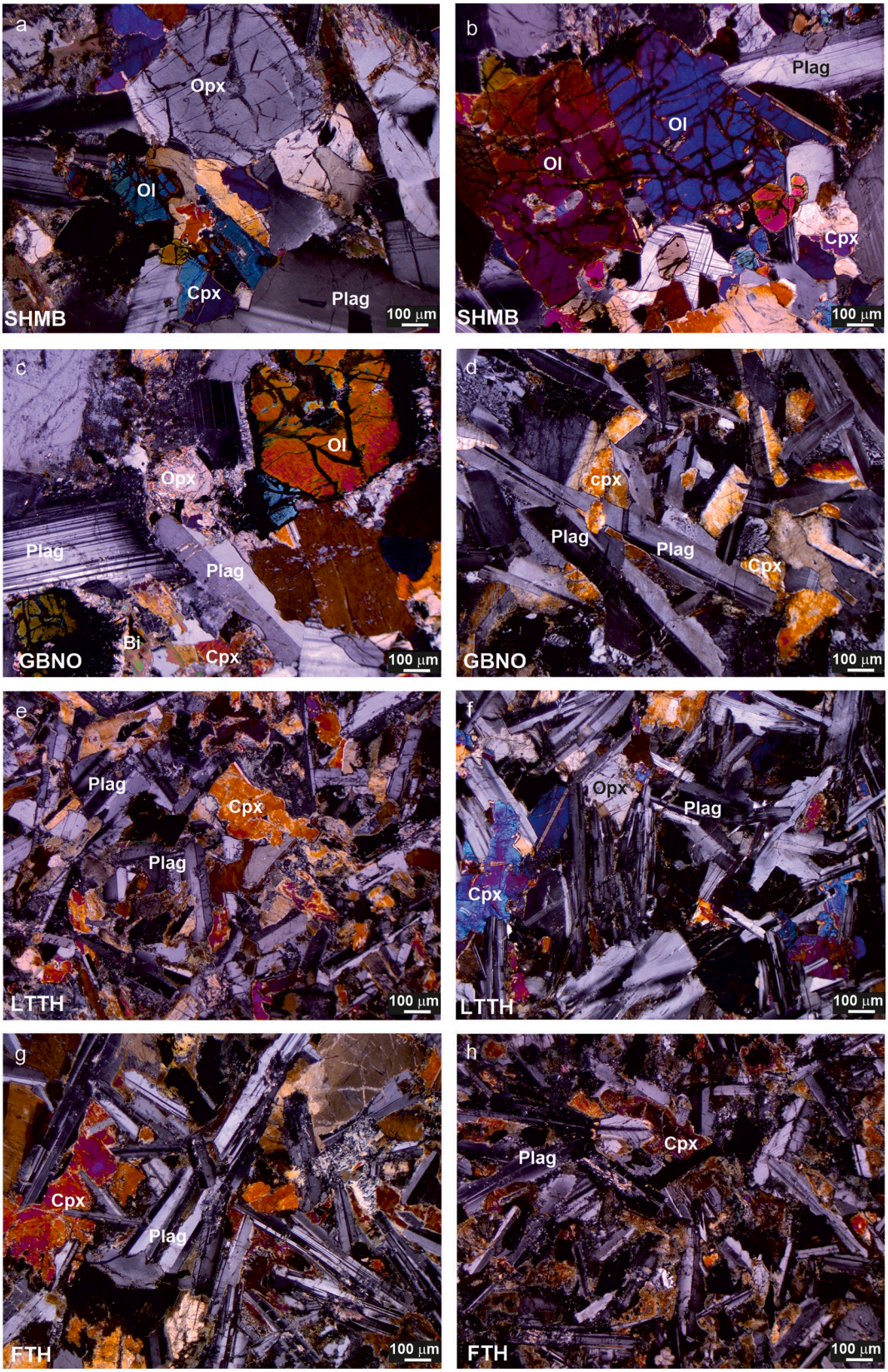

Fig. 3. Photomicrographs (crossed polars) showing the main minerals and textures of the different mafic dyke groups. SHMB = siliceous high-magnesian basalt, GBNO = gabbronorite, LTTH = Low-Ti tholeiite, FTH = Fe-tholeiite. Ol, Cpx, Opx, Plag, Bi indicate olivine, clinopyroxene, orthopyroxene, plagioclase and biotite, respectively.

3. Samples and analytical methods

3.1. Samples

Samples for this study were obtained from a previous project by GTK and University of Oulu (Vuollo and Huhma, 2005), which includes 6 siliceous high magnesian basalts (SHMB), 12 gabbronorites (GBNO), 16 low-Ti tholeiites (LTTH), and 3 Fe-tholeiites (FTH). The SHMB dykes-were mainly collected from the Taivalkoski block, with a few samples also from the Pudasjärvi and Kuhmo blocks in Finland, and Suoperä-Pääjärvi area in Russia. The GBNO dyke samples were mainly collected from the Taivalkoski and Kuhmo blocks. The Low-Ti tholeiitic (LTTH) and Fe-tholeiitic (FTH) dyke samples are from the Taivalkoski block (Fig. 1). The samples were crushed to fragments of about one centimetre in diameter using a steel plate and then pulverised in an agate mill. These methods do not cause elemental contamination, except in minor amounts for Si and O, because the devices were cleaned by crushing quartz between every sample

3.2. Electron microprobe analysis

The compositions of olivine, clinopyroxene, orthopyroxene and plagioclase were determined using a JEOL JXA-8200 electron microprobe at the Centre of Microscopy and Nanotechnology, University of Oulu, using an accelerating voltage of 15 kV and a beam current of 30 nA, which allowed a detection limit of ~150 ppm for some trace elements (e.g., Ni, Cr). The following artificial and natural compounds were used as standards: jadeite for Na, orthoclase for K, wollastonite for Si and Ca, chromite for Cr, oxidic standards for Fe, Mg and Al, and pure metallic standards for V, Mn, Ti, Ni and Zn. The accuracy of the analyses was monitored using reference materials of similar composition. The reproducibility varied by <2% for all reported elements.

3.3. Whole-rock major and trace elements

For most samples, major elements were determined using ICP-OES and a full spectrum of trace elements were determined using ICP-MS (Perkin-Elmer Sciex Elan 5000) at the Cardiff University, UK. For ICP-MS analysis, the samples were dissolved in a mixture of hydrofluoric and perchloric acids in a Teflon dish, evaporated, and redissolved in nitric acid before measurement. To ensure complete decomposition of the samples, the solution was filtered and the filter was ashed and fused with 0.2 g of lithium metaborate and 0.02 g sodium metaborate, followed by dissolution of the fused bead in nitric acid and in combination with the filtrate. This method digests most refractory minerals and provides acceptable precision for all elements. Standard JB1a was used to monitor the analytical quality. The obtained results of these standards are generally consistent with the recommended values, with major elements roughly better than 3%, and trace element 5%, respectively. For a small group of samples, the major elements and selected trace elements (Cr, Ni, Cu, Zr) were determined by XRF at the Geological Survey of Finland (GTK) using a Philips PW 1480 sequential wavelength dispersive spectrometer. The accuracy is better than 2% for element concentrations above 0.5 wt%, 3% for concentrations above 30 ppm, and 5% for concentrations below 30 ppm.

3.4. Platinum-group elements and Au

Platinum-group elements and Au were determined at LabMaTerre, University of Quebec at Chicoutimi (UQAC), using ICP-MS after Ni-sulphide fire assay and tellurium co-precipitation. Analytical details are provided by Savard et al. (2010). To monitor precision and accuracy, PGE and Au were determined for the reference material, OKUM, a komatiite supplied by Geolabs, Ontario (Table 1). The difference between the certificate values and values obtained in this study was 1% to 5% for Ru, Ir, Rh, Pt and Pd, except Au and Os.

3.5. In-situ Sr isotope composition of plagioclase

Pristine plagioclase grains were analysed in situ on thick sections (200 μm) by Laser Ablation ICP-MS using a Nu Plasma HR Multi-collector Inductively Coupled Plasma Mass Spectrometer (MC-ICP-MS) and a Photon Machine Analyte G2 laser microprobe at the Geological Survey of Finland in Espoo. Samples were ablated in He gas (gas flows = 0.4 and 0.1 l/min) within a HelEx ablation cell (Müller et al., 2009). All analyses were made in static ablation mode using a beam diameter of 110 to 200 μm. Details of the analytical procedure are given in Yang et al. (2013). In the course of this study, the $^{87}Sr/^{86}Sr$ ratio of the in-house standard (Mir a) ranged from 0.70309 ± 0.00001 to 0.70318 ± 0.00001, with an average value of 0.70312 ± 0.00003, being within error to the TIMS value of 0.70310 ± 0.00010 (2σ; Rankenburg et al., 2004).

4. Analytical results

4.1. Mineral chemistry

Representative major-element contents of olivine, orthopyroxene, clinopyroxene, and plagioclase are presented in Table 2. Preserved olivine grains mainly occurs in the SHMB dykes. They have Fo contents ranging from 60 to 72 mol%. The olivine grains have relatively high Ni contents (1131–2082 ppm) compared to olivines of similar Fo content in the global database of mafic igneous rocks (Sobolev et al., 2009) (Fig. 4a). This compositional trend resembles that of the Ni-enriched Gudchikhinskaya formation in the Siberian flood basalt sequence (Sobolev et al., 2009), except that olivine grains in our dyke samples are more evolved with lower Fo.

Orthopyroxene could only be analysed in the SHMB and GBNO dykes. The orthopyroxenes in five SHMB samples show relatively high Mg# ranging from 78 to 88 (Fig. 4b). The Mg# values (78–87) of clinopyroxene from SHMB dykes shows a positive correlation with Cr and Ni contents and a negative correlation with Mn and Ti contents. Most clinopyroxenes grains from GBNO dykes have lower Mg# than those from the SHMB dykes, but on the Mg# vs. Cr_2O_3, MnO, and TiO_2

Table 1
Analytical results of platinum group elements standard material Okum in UQAC.

Elements	Detection	Okum UQAC run value		$n = 5$	Okum Certified values		Accuracy %
	Limits (ppb)	Averg. (ppb)	SD	RSD%	Averg. (ppb)	SD	RSD%
Os	0.07	0.69	0.23	33.33	0.98	0.12	12.24
Ir	0.03	0.96	0.16	16.67	0.99	0.07	7.07
Ru	0.12	4.20	0.30	7.14	4.25	0.30	16.47
Rh	0.08	1.34	0.26	19.40	1.40	0.13	9.29
Pt	0.08	11.80	0.50	4.24	11.00	0.60	5.45
Pd	0.47	11.30	0.83	7.35	11.70	0.50	4.27
Au	0.48	1.17	0.34	29.06	1.49	0.16	10.74

Certificate value issued with reference material by International Association of Geoanalysts, except for Os which is from Meisel, 2016.

Table 2
Olivine, orthopyroxene, clinopyroxene and plagioclase composition of different types of 2.45 Ga mafic dykes in Finland.

Sample No.	Rock	SiO_2	TiO_2	Al_2O_3	Cr_2O_3	V_2O_3	FeO	MnO	MgO	CaO	Na_2O	NiO	ZnO	K_2O	Total	Fo
Olivine																
13,3-suo-93,1	SHMB	37.1	0.00	0.00	0.01	0.02	30.5	0.45	31.9	0.15	0.00	0.18	0.06	0.01	100.4	65.0
13,3-suo-93,1,3	SHMB	36.6	0.04	0.02	0.00	0.00	33.3	0.54	30.0	0.14	0.00	0.20	0.06	0.00	101.0	61.6
13,3-suo-93,2,1	SHMB	38.2	0.02	0.03	0.02	0.02	26.8	0.35	35.8	0.15	0.00	0.22	0.00	0.00	101.6	70.5
13,3-suo-93,2,2	SHMB	37.1	0.01	0.00	0.03	0.00	33.4	0.48	30.8	0.10	0.03	0.14	0.03	0.01	102.0	62.2
13,3-suo-93,2,3	SHMB	37.5	0.01	0.05	0.03	0.00	29.0	0.48	33.7	0.20	0.00	0.19	0.00	0.00	101.2	67.4
13,3-suo-93,3,1	SHMB	38.7	0.03	0.02	0.03	0.01	25.1	0.35	37.1	0.15	0.00	0.24	0.08	0.00	101.9	72.5
13,3-suo-93,3,2	SHMB	37.9	0.03	0.01	0.03	0.00	27.9	0.32	35.0	0.19	0.01	0.27	0.01	0.01	101.6	69.1
13,7-suo-93,1,1	SHMB	36.9	0.01	0.01	0.01	0.00	34.8	0.64	28.8	0.22	0.00	0.21	0.02	0.00	101.5	59.6
13,7-suo-93,1,2	SHMB	37.3	0.00	0.01	0.05	0.00	28.4	0.48	31.6	0.11	0.00	0.19	0.00	0.00	98.1	66.5
Orthopyroxene																**Mg#**
13,3-suo-93,1,2	SHMB	57.0	0.08	1.06	0.50	0.00	8.9	0.22	31.3	2.1	0.03	0.07	0.06	0.00	101.3	86.2
13,3-suo-93,1,4	SHMB	57.2	0.09	1.58	0.66	0.02	8.6	0.18	31.7	2.0	0.04	0.10	0.04	0.01	102.3	86.8
13,5-suo-93,1,1	SHMB	56.3	0.10	1.97	0.87	0.02	8.1	0.17	31.8	1.9	0.06	0.15	0.06	0.02	101.6	87.4
13,5-suo-93,1,2	SHMB	55.8	0.08	1.48	0.19	0.00	11.4	0.25	29.4	2.3	0.05	0.05	0.03	0.02	101.0	82.1
13,5-suo-93,3,1	SHMB	55.7	0.10	1.87	0.81	0.02	9.0	0.20	30.6	2.5	0.05	0.05	0.03	0.00	101.1	85.8
13,7-suo-93,cpx,4,2	SHMB	55.7	0.13	2.03	0.78	0.02	10.2	0.23	28.6	1.9	0.08	0.06	0.03	0.06	99.9	83.3
13,3-suo-93,opx,3,10	SHMB	56.4	0.07	1.58	0.63	0.01	7.6	0.23	30.7	2.1	0.05	0.02	0.00	0.00	99.4	87.8
13,3-suo-93,opx,3,11	SHMB	56.2	0.06	1.80	0.85	0.01	8.3	0.19	31.2	2.0	0.00	0.10	0.03	0.01	100.7	87.1
9-suo-92,1,2	SHMB	39.2	0.00	0.02	0.03	0.05	19.6	0.32	39.0	0.2	0.00	0.26	0.05	0.00	98.8	78.0
9-suo-92,1,9	SHMB	55.0	0.11	2.14	0.67	0.02	8.7	0.24	29.5	2.5	0.05	0.04	0.03	0.00	99.1	85.8
O332,2,1	SHMB	55.9	0.11	1.12	0.35	0.00	9.1	0.30	29.2	2.3	0.10	0.02	0.02	0.00	98.5	85.1
O332,2,3	SHMB	55.5	0.10	1.54	0.35	0.00	9.7	0.22	29.2	2.3	0.06	0.07	0.00	0.01	98.9	84.3
Clinopyroxene																**Mg#**
13,3-suo-93	SHMB	52.9	0.21	2.87	0.83	0.05	6.5	0.22	19.0	17.5	0.28	0.06	0.00	0.01	100.5	83.9
13,3-suo-93	SHMB	52.5	0.38	2.20	0.03	0.07	10.3	0.28	18.1	15.7	0.24	0.04	0.00	0.00	99.8	75.8
13,5-suo-93	SHMB	52.6	0.29	2.46	0.10	0.00	8.5	0.25	18.0	17.7	0.27	0.00	0.08	0.00	100.3	79.1
13,5-suo-93	SHMB	51.4	0.71	2.81	0.03	0.10	12.4	0.32	15.0	17.7	0.39	0.04	0.00	0.00	100.9	68.4
13,7-suo-93	SHMB	53.1	0.14	2.03	0.10	0.00	8.2	0.25	18.6	16.2	0.21	0.00	0.06	0.01	99.0	80.1
13,7-suo-93	SHMB	53.2	0.20	2.15	0.08	0.03	8.7	0.21	17.8	16.7	0.26	0.04	0.00	0.00	99.5	78.5
13,5-suo-93	SHMB	51.5	0.50	2.82	0.05	0.09	11.9	0.34	14.8	17.6	0.43	0.04	0.04	0.00	100.1	68.9
13,5-suo-93	SHMB	52.9	0.19	2.47	0.09	0.02	8.9	0.15	17.1	16.3	0.27	0.07	0.00	0.02	98.5	77.3
13,3-suo-93	SHMB	53.1	0.26	2.34	0.08	0.04	7.7	0.24	18.3	15.7	0.26	0.11	0.06	0.00	98.1	80.9
13,3-suo-93	SHMB	53.2	0.16	2.72	0.52	0.05	6.2	0.18	18.2	18.0	0.31	0.06	0.00	0.00	99.4	84.0
9-suo-92	SHMB	53.2	0.25	2.56	0.23	0.01	7.0	0.22	17.9	17.8	0.25	0.08	0.00	0.00	99.5	82.0
9-suo-92	SHMB	52.9	0.28	2.73	0.11	0.04	7.7	0.20	17.7	17.0	0.20	0.03	0.06	0.00	98.9	80.4
9-suo-92	SHMB	52.8	0.23	2.83	0.57	0.03	6.0	0.17	18.4	17.4	0.24	0.06	0.03	0.00	98.7	84.6
O332,2,2	SHMB	53.2	0.29	2.38	0.41	0.07	7.3	0.20	17.7	18.5	0.34	0.10	0.02	0.00	100.5	81.2
O332,2,5	SHMB	53.1	0.16	2.37	0.90	0.01	5.4	0.16	18.2	19.0	0.25	0.02	0.01	0.01	99.7	85.7
O332,2,6	SHMB	53.0	0.18	2.62	0.92	0.01	5.2	0.19	18.6	18.9	0.18	0.07	0.11	0.00	99.9	86.5
19-SUO-93	GBNO	53.4	0.26	2.88	0.42	0.06	7.6	0.18	17.9	18.0	0.30	0.09	0.06	0.00	101.2	80.7
19-SUO-93	GBNO	52.4	0.28	2.45	0.17	0.06	8.5	0.25	17.8	16.6	0.24	0.04	0.00	0.00	98.7	79.0
19-SUO-93	GBNO	52.1	0.22	3.56	0.93	0.09	5.6	0.19	18.0	18.1	0.32	0.05	0.02	0.02	99.2	85.2
122-VEN-94	GBNO	51.0	0.38	2.62	0.00	0.04	11.9	0.32	14.5	16.9	0.35	0.00	0.13	0.01	98.2	68.4
122-VEN-94	GBNO	51.1	0.35	2.58	0.01	0.08	12.9	0.33	14.4	16.6	0.39	0.01	0.08	0.00	98.8	66.5
122-VEN-94	GBNO	51.7	0.31	2.53	0.08	0.05	10.0	0.22	15.6	17.7	0.34	0.00	0.09	0.00	98.6	73.6
122-VEN-94	GBNO	52.4	0.31	2.10	0.27	0.04	8.8	0.23	16.9	17.3	0.25	0.00	0.00	0.00	98.5	77.4
122-VEN-94	GBNO	51.0	0.30	2.42	0.03	0.03	10.2	0.30	15.5	17.4	0.30	0.00	0.00	0.00	97.5	73.0
AD14-2	GBNO	51.0	0.72	3.18	0.02	0.08	13.5	0.35	14.8	16.6	0.33	0.05	0.00	0.01	100.7	66.2
AD14-2	GBNO	51.3	0.64	3.12	0.05	0.02	8.3	0.30	15.6	19.3	0.25	0.00	0.00	0.00	98.8	77.0
AD14-2	GBNO	51.3	0.53	2.71	0.06	0.06	8.3	0.28	15.9	18.9	0.25	0.00	0.00	0.00	98.3	77.4
AD14-2	GBNO	50.9	0.84	3.56	0.15	0.07	7.1	0.20	15.2	20.1	0.27	0.02	0.05	0.00	98.5	79.1
Plagioclase																**An#**
13,3-suo-93,1,5	SHMB	55.5	0.07	28.21	0.00	0.00	0.6	0.00	0.1	10.9	5.55	0.01	0.01	0.31	101.2	52
13,3-suo-93,3,5	SHMB	53.2	0.05	29.39	0.02	0.00	0.4	0.00	0.1	12.3	4.59	0.02	0.03	0.29	100.4	60
13,3-suo-93,plg,3,8	SHMB	52.9	0.03	29.51	0.02	0.00	0.3	0.01	0.1	12.6	4.58	0.00	0.08	0.11	100.2	60
13,5-suo-93,3,4	SHMB	52.9	0.07	29.63	0.00	0.00	0.5	0.00	0.2	12.7	4.56	0.05	0.00	0.31	100.8	61
13,5-suo-93,plg,4,3	SHMB	53.1	0.02	29.91	0.00	0.00	0.4	0.00	0.1	13.0	4.42	0.00	0.05	0.19	101.2	62
13,5-suo-93,plg,4,4	SHMB	53.9	0.02	29.64	0.00	0.00	0.4	0.01	0.1	12.6	4.71	0.00	0.07	0.12	101.5	60
13,5-suo-93,plg,4,5	SHMB	51.5	0.02	30.64	0.00	0.00	0.4	0.00	0.2	13.4	4.16	0.06	0.00	0.10	100.4	64
13,7-suo-93,3,3	SHMB	54.6	0.05	29.04	0.00	0.01	0.6	0.02	0.1	11.8	5.20	0.00	0.00	0.13	101.5	56
13,7-suo-93,plg,4,5	SHMB	52.7	0.05	29.59	0.00	0.03	0.4	0.01	0.2	12.8	4.50	0.00	0.00	0.17	100.4	61
13,7-suo-93,plg,3,4	SHMB	54.3	0.02	28.86	0.00	0.00	0.4	0.03	0.1	11.9	5.30	0.01	0.00	0.09	101.1	56
13,7-suo-93,plg,3,5	SHMB	53.3	0.04	29.48	0.00	0.00	0.4	0.01	0.1	12.7	4.65	0.00	0.03	0.12	100.8	60
9-suo-92,1,6	SHMB	51.5	0.01	30.87	0.01	0.00	0.4	0.00	0.1	14.2	3.86	0.00	0.00	0.15	101.1	67
9-suo-92,1,8	SHMB	53.0	0.01	30.10	0.04	0.00	0.4	0.01	0.1	13.4	4.22	0.04	0.00	0.21	101.6	64
O332,2,4	SHMB	54.2	0.04	29.05	0.00	0.00	0.6	0.04	0.1	11.8	4.86	0.02	0.08	0.34	101.2	57
O332,2,7	SHMB	52.5	0.01	30.21	0.00	0.00	0.6	0.04	0.1	13.0	4.19	0.01	0.00	0.04	100.7	63
O332,2,8	SHMB	51.6	0.02	30.89	0.00	0.02	0.6	0.01	0.1	13.8	4.10	0.00	0.07	0.06	101.2	65
17-suo-93-plg-1,1	GBNO	58.5	0.05	26.15	0.01	0.02	0.2	0.00	0.0	8.0	7.50	0.01	0.04	0.06	100.7	37
17-suo-93-plg-1,2	GBNO	53.3	0.03	29.81	0.02	0.00	0.6	0.01	0.1	12.2	4.86	0.00	0.00	0.16	101.1	58
17-suo-93-plg-1,4	GBNO	53.5	0.03	29.45	0.00	0.00	0.6	0.01	0.1	12.5	4.81	0.04	0.00	0.17	101.1	59
17-suo-93-plg-1,5	GBNO	55.5	0.07	28.19	0.00	0.01	0.6	0.02	0.1	10.6	5.94	0.00	0.08	0.20	101.4	50
19-SUO-93-1,1	GBNO	52.8	0.03	29.29	0.00	0.00	0.5	0.00	0.1	12.6	4.41	0.03	0.01	0.36	100.1	61

(*continued on next page*)

Table 2 (*continued*)

Sample No.	Rock	SiO_2	TiO_2	Al_2O_3	Cr_2O_3	V_2O_3	FeO	MnO	MgO	CaO	Na_2O	NiO	ZnO	K_2O	Total	Fo
19-SUO-93-1,3	GBNO	54.5	0.05	28.84	0.00	0.00	0.5	0.01	0.1	11.5	5.16	0.00	0.00	0.43	101.2	55
19-SUO-93-1,4	GBNO	56.1	0.09	27.54	0.00	0.02	0.5	0.04	0.1	10.2	5.67	0.00	0.15	0.63	100.9	50
19-SUO-93-1,8	GBNO	55.2	0.06	28.24	0.00	0.00	0.6	0.01	0.1	11.4	5.22	0.01	0.00	0.46	101.3	55
19-SUO-93-1,9	GBNO	55.0	0.05	28.54	0.00	0.02	0.5	0.02	0.1	11.4	5.29	0.00	0.09	0.38	101.4	55
122-VEN-94-1,1	GBNO	57.7	0.01	27.00	0.00	0.00	0.6	0.02	0.1	9.1	6.68	0.00	0.03	0.18	101.5	43
122-VEN-94-plag-1,8	GBNO	52.0	0.03	29.20	0.02	0.00	0.8	0.02	0.2	12.0	4.30	0.01	0.00	0.43	99.1	61
122-VEN-94-plag-1,9	GBNO	55.2	0.04	28.29	0.02	0.00	0.5	0.00	0.0	11.4	5.51	0.00	0.05	0.28	101.4	54
122-VEN-94-plag-1,10	GBNO	53.6	0.00	28.38	0.01	0.00	0.6	0.00	0.0	11.2	5.24	0.00	0.09	0.27	99.5	54
122-VEN-94-plag-1,11	GBNO	54.7	0.05	25.30	0.03	0.00	2.3	0.03	1.0	8.1	5.93	0.02	0.01	0.37	97.9	43
AD54-1-plag-1,3	GBNO	52.3	0.02	29.71	0.01	0.00	0.5	0.00	0.1	12.8	4.73	0.04	0.03	0.09	100.3	60
AD54-1-plag-1,4	GBNO	56.6	0.03	27.86	0.00	0.00	0.2	0.01	0.1	7.8	6.60	0.00	0.01	0.68	99.9	40
AD54-1-plag-1,5	GBNO	53.0	0.04	29.72	0.01	0.00	0.3	0.00	0.0	12.5	4.95	0.00	0.00	0.06	100.6	58
122-VEN-94-4,1	GBNO	54.8	0.03	28.75	0.02	0.00	0.5	0.00	0.0	11.3	5.48	0.00	0.03	0.11	101.0	53
122-VEN-94-4,3	GBNO	56.0	0.04	27.51	0.00	0.03	0.5	0.00	0.1	10.2	5.96	0.00	0.07	0.36	100.8	49
AD54-1-1,2	GBNO	53.8	0.04	29.04	0.00	0.04	0.4	0.02	0.1	11.7	5.46	0.00	0.03	0.03	100.7	54
AD14-2-1,8	GBNO	52.6	0.07	28.79	0.04	0.00	1.0	0.00	0.1	11.9	4.06	0.00	0.10	1.05	99.7	62
AD14-2-1,9	GBNO	54.6	0.03	28.48	0.00	0.01	0.5	0.03	0.1	11.5	5.22	0.04	0.00	0.29	100.8	55
AD14-2-plag-1,10	GBNO	54.2	0.05	28.06	0.00	0.00	0.6	0.03	0.1	11.5	5.30	0.04	0.08	0.31	100.3	55
AD14-2-plag-1,11	GBNO	52.9	0.04	29.26	0.04	0.00	0.6	0.00	0.1	12.7	4.74	0.00	0.00	0.16	100.5	60
AD14-2-plag-1,12	GBNO	52.6	0.06	29.85	0.00	0.02	0.6	0.00	0.1	13.1	4.29	0.00	0.05	0.23	100.9	63
AD3-2-1,1	LTTH	54.3	0.04	28.05	0.00	0.00	0.7	0.02	0.1	11.6	5.15	0.00	0.03	0.25	100.2	56
AD3-2-1,2	LTTH	56.2	0.04	26.60	0.00	0.01	0.6	0.00	0.0	9.9	6.14	0.00	0.00	0.37	99.9	47
AD3-2-1,3	LTTH	53.8	0.04	28.95	0.05	0.00	0.6	0.03	0.1	11.8	4.92	0.00	0.00	0.23	100.6	57
AD3-2-1,4	LTTH	53.3	0.04	28.48	0.01	0.00	0.7	0.05	0.1	12.3	4.80	0.01	0.03	0.20	100.0	59
AD3-2-1,5	LTTH	52.7	0.05	28.47	0.00	0.00	0.6	0.03	0.1	12.1	4.68	0.00	0.04	0.24	99.0	59
1-UD-93-1,1	LTTH	56.0	0.02	28.06	0.01	0.00	0.2	0.00	0.0	10.1	6.25	0.00	0.00	0.13	100.8	47
1-UD-93-1,3	LTTH	60.2	0.03	26.78	0.00	0.04	0.1	0.01	0.0	8.0	7.62	0.00	0.05	0.13	102.9	37
1-UD-93-1,4	LTTH	55.6	0.03	27.84	0.01	0.00	0.7	0.00	0.1	10.8	5.81	0.00	0.00	0.16	101.0	51
1-UD-93-1,5	LTTH	53.7	0.04	28.93	0.00	0.00	0.4	0.00	0.1	12.3	4.99	0.00	0.08	0.13	100.7	58
1-UD-93-1,6	LTTH	54.4	0.04	28.05	0.00	0.00	0.7	0.00	0.1	11.0	5.67	0.03	0.02	0.14	100.1	52
1-UD-93-1,7	LTTH	54.6	0.05	28.36	0.04	0.00	0.6	0.01	0.1	11.6	5.30	0.02	0.04	0.12	100.9	55
WD11-1,1	FTH	53.4	0.07	29.31	0.01	0.00	0.6	0.00	0.1	12.6	4.80	0.00	0.00	0.20	101.1	59
WD11-1,3	FTH	52.2	0.07	29.75	0.00	0.00	0.6	0.00	0.1	13.3	4.31	0.00	0.00	0.14	100.5	63
WD11-1,4	FTH	54.9	0.11	28.00	0.05	0.02	0.7	0.04	0.1	11.2	5.38	0.01	0.09	0.31	100.9	54
WD11-1,5	FTH	53.5	0.08	29.59	0.05	0.01	0.6	0.00	0.2	11.9	4.41	0.00	0.00	0.64	100.9	60
WD11-1,6	FTH	52.4	0.07	29.96	0.00	0.06	0.5	0.01	0.1	13.0	4.38	0.00	0.00	0.08	100.6	62
WD12-1,1	FTH	52.4	0.04	29.73	0.03	0.00	0.6	0.00	0.2	13.2	4.33	0.00	0.00	0.09	100.7	63
WD12-1,2	FTH	52.0	0.02	30.21	0.05	0.00	0.5	0.00	0.1	13.7	4.04	0.02	0.00	0.12	100.8	65
WD12-1,3	FTH	52.0	0.04	30.26	0.00	0.01	0.5	0.00	0.2	14.0	3.77	0.00	0.00	0.10	100.9	67
WD12-1,4	FTH	56.7	0.10	27.09	0.04	0.03	0.5	0.00	0.1	9.9	6.22	0.00	0.00	0.36	100.9	47
WD12-1,5	FTH	54.1	0.08	28.80	0.01	0.00	0.5	0.00	0.1	12.5	4.93	0.00	0.02	0.17	101.3	58
WD13-1,1	FTH	51.2	0.07	29.64	0.01	0.00	0.5	0.00	0.1	13.4	4.01	0.00	0.04	0.14	99.1	65
WD13-1,2	FTH	52.0	0.04	29.75	0.00	0.00	0.6	0.00	0.1	13.1	4.31	0.00	0.03	0.10	99.9	63
WD13-1,3	FTH	54.7	0.06	27.58	0.03	0.00	0.5	0.00	0.1	10.7	5.73	0.01	0.00	0.23	99.5	51
WD13-1,4	FTH	53.9	0.08	28.01	0.00	0.02	0.5	0.01	0.1	11.4	5.24	0.01	0.00	0.13	99.4	55
WD13-1,5	FTH	53.1	0.06	28.67	0.01	0.02	0.5	0.02	0.2	12.2	4.84	0.05	0.03	0.20	99.9	58
WD13-1,6	FTH	55.9	0.11	26.57	0.00	0.00	0.4	0.04	0.1	9.6	6.19	0.00	0.05	0.32	99.3	46
WD14-1,1	FTH	54.3	0.06	27.99	0.00	0.00	0.6	0.02	0.1	10.9	5.41	0.00	0.00	0.24	99.7	53
WD14-1,2	FTH	56.5	0.05	27.21	0.00	0.00	0.4	0.04	0.0	9.8	6.32	0.06	0.04	0.37	100.9	46
WD14-1,3	FTH	52.5	0.04	29.63	0.08	0.00	0.4	0.05	0.1	13.0	4.51	0.02	0.00	0.06	100.4	61
WD14-1,4	FTH	52.6	0.06	29.83	0.00	0.03	0.4	0.00	0.1	13.3	4.03	0.02	0.00	0.10	100.6	65
WD14-1,5	FTH	53.0	0.06	29.43	0.02	0.00	0.4	0.02	0.1	12.8	4.59	0.00	0.00	0.14	100.7	61

diagrams, GBNO clinopyroxene plots on the same trends as those of the SHMB samples (Fig. 5). Moreover, when the clinopyroxene compositions of the dykes are compared with those from the Penikat intrusion, it is apparent that both populations define similar compositional trends, though a few samples of the megacyclic unit V of the Penikat intrusion show a slightly higher Ti content.

Plagioclase was analysed from all dyke types. The grains from the SHMB dykes have a restricted An content from 52 to 67 mol%. The An content of the analysed GBNO plagioclase grains shows slightly lower values but wider range from 37 to 61 mol%. Plagioclase grains in the LTTH dykes have An contents ranging from 37 to 59 mol%, and plagioclase grains in the FTH dykes have 46 to 67 mol% An (Table 2).

4.2. Major and lithophile trace elements

The SHMB and GBNO dykes have broadly similar major element compositions, displaying good overlap on binary variation diagrams (Supplementary table 1, Fig. 6). The SHMB dykes display a somewhat wider compositional range than the GBNO dykes. The former has 4.6–18.4 wt% MgO, 52–57 wt% SiO_2, 2–4.5 wt% $Na_2O + K_2O$, 11–2376 ppm Cr, and 78.5–894 ppm Ni, while the latter have 5.41–13.7 wt% MgO, 51–56 wt% SiO_2, 1.5–3.2 wt% $Na_2O + K_2O$, 67.6–1293 ppm Cr, and 43.9–371 ppm Ni. One striking feature of these two dyke groups is the relatively high SiO_2 and alkali ($Na_2O + K_2O$) contents at a given MgO content (Fig. 6).

The LTTH dykes have 4–9 wt% MgO, 47–53 wt% SiO_2, and 2.01–3.86 wt% $Na_2O + K_2O$, 263.5–277.8 ppm Cr, 121–143 ppm Ni. Due to the relatively small number of samples, the FTH dykes show a limited variation in the binary variation diagrams. The samples contain 48.5–49.5 wt% SiO_2, 5.79–6.23 wt% MgO, 2.6–2.7 wt% $Na_2O + K_2O$, 263.5–277.8 ppm Cr, 121–143 ppm Ni, and plot broadly together with the LTTH dykes (Fig. 6). The two groups of tholeiite dykes show clearly lower SiO_2 and alkali contents, and also lower Cr and Ni contents, but slightly higher FeO contents than the SHMB and GBNO groups. It is worth noting that in terms of major elements and also Cr and Ni, the B1 type magma of the Bushveld plot in the same field as the SHMB and

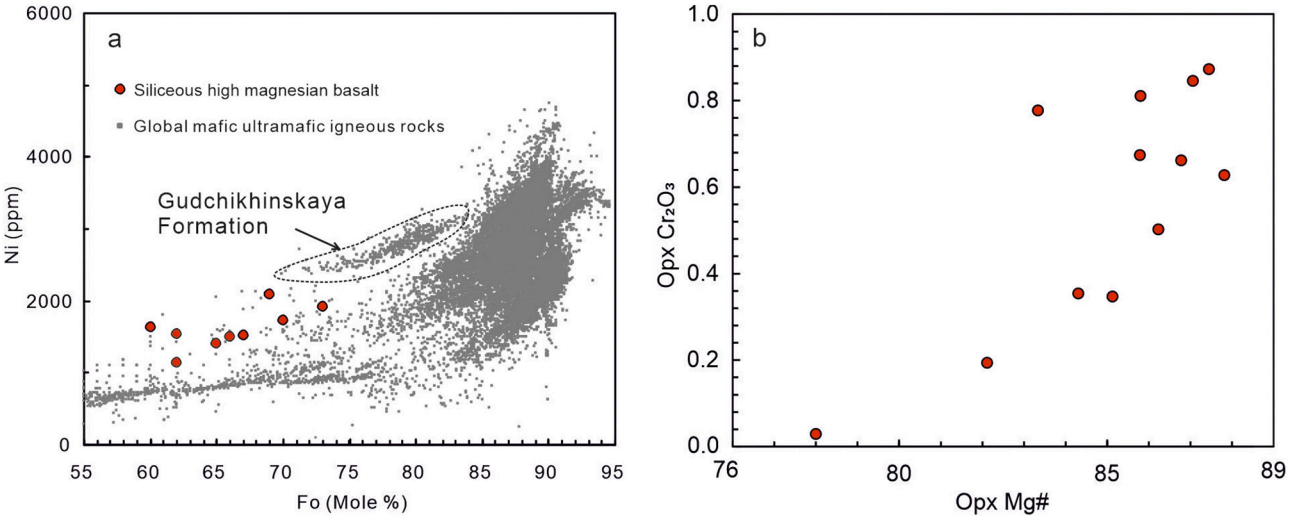

Fig. 4. Mineral compositions from SHMB dykes. A. Fo and Ni contents of olivine compared with data from a global olivine database. Global data taken from (Sobolev et al., 2009). B. Mg# vs. Cr_2O_3 for orthopyroxene.

GBNO groups, and the B2 and B3 rocks of the Bushveld in the field of the LTTH and FTH dyke groups (Fig. 6).

The SHMB and GBNO suites generally have low Ti contents, with Ti falling below 6000 ppm (or < 1% TiO_2). The LTTH and FTH dykes have clearly higher TiO_2 (2.47–2.61 wt%) than the SHMB and GBNO dykes (Figs. 6c, 7a). However, all dyke groups mainly plot in the field of the low-Ti series of other LIPs, though the FTH group plots near the lower range of the high-Ti series (e.g., Emeishan, Paraná, Fig. 7a) (Arguin et al., 2016; Mansur et al., 2021). This is consistent with the observation that all mafic dyke groups in Fennoscandia show lower Ti/Y ratios than the high-Ti series in other LIPs (Fig.7b). Compared with the high-Ti series of the Emeishan and Paraná flood basalts, the dykes in Fennoscandia show lower Sm/Yb and La/Yb ratios (Figs. 7c, d).

The SHMB and GBNO dykes display fractionated chondrite-normalised REE patterns with a clear enrichment in LREE compared to HREE (Figs. 8a, b). One of the tholeiitic dykes shows a flat REE pattern, whereas the majority of the tholeiitic samples show enrichment in LREE but with less fractionated LREE/HREE compared to the SHMB and GBNO dykes (Figs. 8c, d). Notably, among the tholeiites, the Fe tholeiites show small negative Eu anomalies, but this is not a characteristic feature of all LTTH dykes.

In primitive mantle-normalised incompatible trace element plots, both SHMB and GBNO dykes show strong negative Ta—Nb and P anomalies, and relative enrichments in Rb, Ba, Th, U and Pb, whereas the tholeiitic dykes display weak negative Ta—Nb anomalies and generally rather flat patterns, albeit with minor enrichment in Pb and depletions in K, Sr and P (Fig. 8e, h). The FTH group shows strong negative Sr anomalies, which is consistent with the negative Eu anomalies of this dyke type. All dyke samples show a negative correlation between Nb/La and La/Sm ratios and a positive correlation between Ce/Yb and La/Sm ratios (Fig. 9), suggesting the presence of a crustal component, especially in the SHMB and GBNO suites, and to be discussed in more detail later.

4.3. Chalcophile elements

Chalcophile elements data for different dyke types are listed in Table 3. The SHMB dykes have rather variable Pt and Pd contents, ranging from 0.24 to 12.0 ppb, and contain 0.72 to 3.84 ppb Rh, 0.02–0.89 ppb Ir, 0.2–5.84 ppb Ru, 22–152 ppm Cu and 0.24–1.8 ppb Au (Table 4). The GBNO samples have broadly similar chalcophile element concentrations to those of the SHMB samples. In the SHMB and GBNO groups, MgO have good positive correlations with Ir, Ru and Rh, but a poor correlation with Pt, Pd, Au. However, the most primitive samples with MgO from 15 to 20 wt% show moderate Pt and Pd contents ranging from 5 to 10 ppb, and the highest Pt and Pd contents occur in samples with moderate MgO of about 10 wt% (Fig. 10). Samples with low MgO contents (4–7 wt%) display a large variation in Pt and Pd contents, varying from values below the detection limit to the highest values found in the entire dyke population (Fig. 10). The LTTH dykes also have variable Pt and Pd contents ranging from 0.24 to 24.3 ppb, and very low Ir and Ru contents from below detection limit to 0.21 ppb, and 0.04–0.52 ppb Rh, 81.2–254 ppm Cu and 0.24–7.66 ppb Au (Table 4). The FTH dykes have narrow range of 11.0–14.2 ppb for Pt and Pd, 1–1.3 ppb Rh, low Ir contents from 0.12 to 0.14 ppb, low Ru contents from 0.63 to 0.72 ppb, and 13–76 ppm Cu, and 0.89–2.7 ppb Au (Table 4). Some samples of the LTTH group with moderate MgO contents (5–9 wt %) show the highest Pd and Pt contents of up to 24 ppb and 20 ppb, respectively, being higher than in the SHMB and GBNO groups. Other samples with lower MgO contents (4–7 wt%) have very low Pd and Pt contents falling below the detection limit. In contrast, the LTTH dykes show relatively low IPGE and Rh contents (Fig. 10). The FTH group with a limited number of samples (3) have moderate Pd and Pt contents, similar to those of the SHMB and GBNO dykes, and low but detectable IPGE contents, overlapping with the positive trend between IPGE and MgO displayed by the SHMB and GBNO groups. However, the FTH dykes show the highest Cu content of about 300 ppm among all dyke groups (Fig. 11). For all four dyke groups, the variation in Au is similar to that of Pd and Pt, though more scattered (Fig. 10). Platinum shows a positive correlation with Pd, plotting broadly on the 1:1 trend line, although some LTTH samples show higher Pd than Pt (2:1) (Fig. 11). This trend is somehow different from the Bushveld magma compositions (B1, B2, B3), which have higher Pt/Pd ratios (Fig. 11). On the plot of Ir vs. Pt, the SHMB and GBNO dykes show relatively high Ir and moderate Pt contents, and some LTTH and FTH dykes show low Ir but high Pt contents, whereas the other samples display very low Pt and Ir contents. In this plot, the B1 marginal rocks from Bushveld display a lot of overlap with the SHMB and GBNO group dykes, and the B2 and B3 rocks with the LTTH and FTH groups.

The samples of all four dyke groups show mostly PGE-undepleted primitive mantle-normalised chalcophile element patterns, except that the IPGE are generally depleted relative to Ni, and Au is depleted relative to Pd and Cu (Fig. 12). In terms of chalcophile element patterns, the SHMB and GBNO groups are similar to Bushveld B1, and the LTTH and FTH groups similar to Bushveld B2 and B3. Accordingly, the FTH samples typically have very high Cu/Pd >20,000 whereas most samples

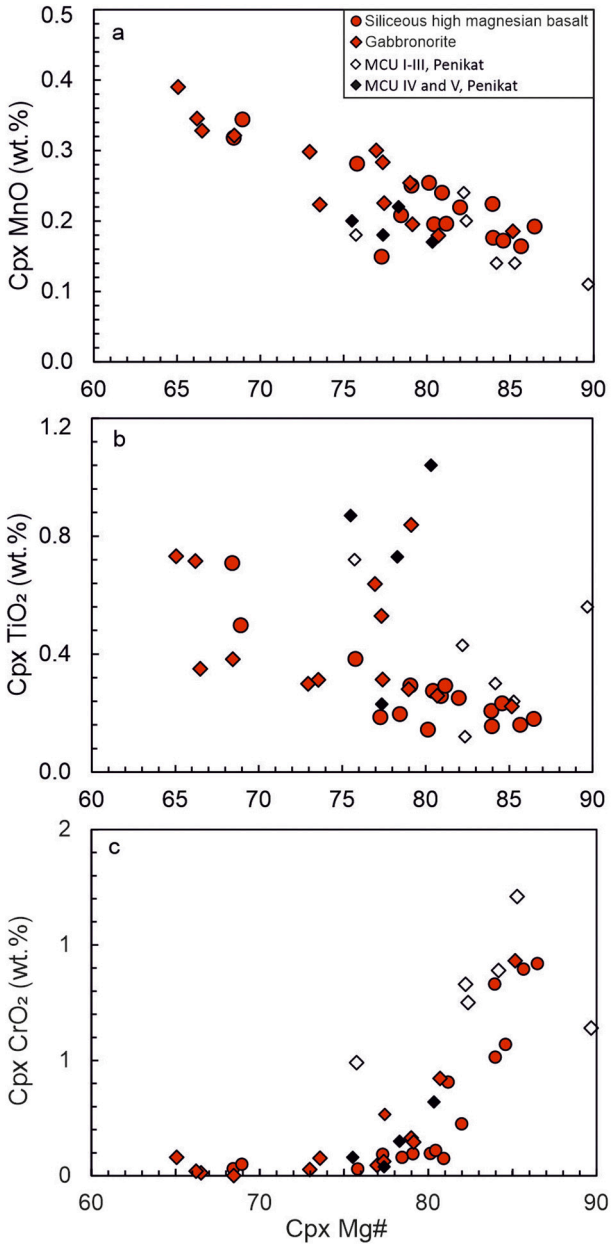

Fig. 5. Clinopyroxene compositions from SHMB and GBNO dykes compared with data from five megacyclic units of the Penikat intrusion. Penikat data taken from (Alapieti and Halkoaho, 1995).

from the other groups have Cu/Pd <15,000, except a couple of LTTH and GBNO samples with low Pd contents below detection limit showing the highest Cu/Pd ratios (Fig. 11).

4.4. Sr isotopes

The Sr isotope composition was determined for plagioclase from 14 dyke samples, with 5–13 grains for each sample (Table 5). The SHMB and GBNO dykes share similar Sr isotope compositions with each other by having initial $^{87}Sr/^{86}Sr$ ratios of about 0.7030, which is clearly higher than the depleted mantle value of about 0.7010 at 2.45 Ga (Amelin and Semenov, 1996). The tholeiitic dykes show a lower initial $^{87}Sr/^{86}Sr$ value of about 0.7022, being only slightly higher than the depleted mantle composition (Table 5, Fig. 13). These data are consistent with the negative initial εNd values of the SHMB and GBNO dykes and the positive initial εNd values of the tholeiitic dykes (Fig. 13), demonstrating different degrees of source enrichment or crustal contamination in these dyke groups. It is interesting that the SHMB and GBNO samples with the highest initial $^{87}Sr/^{86}Sr$ ratios also show the largest intra-sample variation in initial $^{87}Sr/^{86}Sr$. This is in line with the general large variation of initial εNd values (Fig. 13). Similar large intra-sample variation of initial $^{87}Sr/^{86}Sr$ has been observed in mafic intrusions affected by crustal contamination in the Musgrave province in Australia (Maier et al., 2015)

5. Discussion

5.1. Mantle sources of the dyke groups

The nature of the mantle source to the 2.45 Ga magmatism in the Karelian craton remains under debate. Based on Nd isotope data from layered intrusions, Amelin and Semenov (1996) proposed that the parental magmas to the intrusions were derived from a mantle plume and underwent small to moderate amounts (4–20%) of contamination during their ascent to the upper crust. This model is consistent with Os and Nd isotope data from the 2.45 Ga Koitelainen and Akanvaara intrusions (Hanski et al., 2001). However, as an alternative interpretation, the magmas could have formed through melting of metasomatically modified subcontinental lithospheric mantle (SCLM) (Amelin and Semenov, 1996; Huhma et al., 1990).

The available isotope and lithophile trace element data from the dyke suites provide new constraints on these models. The SHMB and GBNO dykes have negative initial εNd values (from −2.5 to −1.0), relatively high initial $^{87}Sr/^{86}Sr$ ratios (07028–0.7036) (Fig. 13), and negative Ta—Nb anomalies in multi-element variation plots. They also have relatively high La/Sm and Ce/Yb and low Nb/La ratios (Fig. 10). We argue that these data are more readily explained by crustal contamination of asthenospheric magma than melting of SCLM for the following reasons. First, magmas derived from the SCLM would be expected to mix efficiently during ascent through the SCLM, resulting in a relatively constant enriched geochemical composition (Arndt, 2013 and references therein). In Fennoscandia, the lithophile trace element composition of the SHMB and GBNO dykes is highly heterogenous, showing an up to 3-fold variation. In addition, La/Sm displays a strong positive correlation with Ce/Yb and a negative correlation with Nb/La, consistent with variable degrees of crustal contamination (Fig. 10). Similar variation has been reported for coeval komatiites in the Vetreny belt (Puchtel et al., 1996) and interpretated as a result of AFC processes affecting a komatiitic magma derived from a mantle plume. In fact, our SHMB and GBNO dykes display much larger compositional variation, with the Vetreny belt komatiites plotting near the lower end of the variation trend (Fig. 10). This feature suggests that the Vetreny komatiite experienced less crustal contamination compared to our SHMB and GBNO dyke magmas. We conducted a simplified two component mixing model between an Archaean komatiitic magma and crust. Based on the Al-undepleted nature of the Vetreny komatiite, the komatiitic magma is assumed to be similar in composition to the komatiite in Belingwe (24 wt% MgO, Shimizu et al., 2005). With regard to the crustal end member, we tested two options: ~2.8 Ga trondhjemite, which occurs widely in the Karelian craton, and ~ 2.7 Ga granite, which is proposed to represent a partial melt of trondhjemite (Mikkola et al., 2011). It is quite possible that the komatiitic magma triggered partial melting, but not bulk melting, of the crustal rocks, hence the composition of the 2.7 Ga granite is used as a crustal-end member. The modelling results indicate that the SHMB and GBNO dykes underwent variable degrees of crustal contamination ranging from 3 to 5 wt%, whereas the Vetreny komatiite underwent contamination of about 2 wt % (Fig. 9).

Compared with the SHMB and GBNO dykes, the LTTH and FTH dykes exhibit no or weaker Ta—Nb anomalies, higher initial εNd values (from −0.3 to +1.7) (Vuollo and Huhma, 2005), and lower initial $^{87}Sr/^{86}Sr$ ratios (~0.7022) (Fig. 13). These features are best interpreted to be derived from a long-term depleted asthenospheric mantle component,

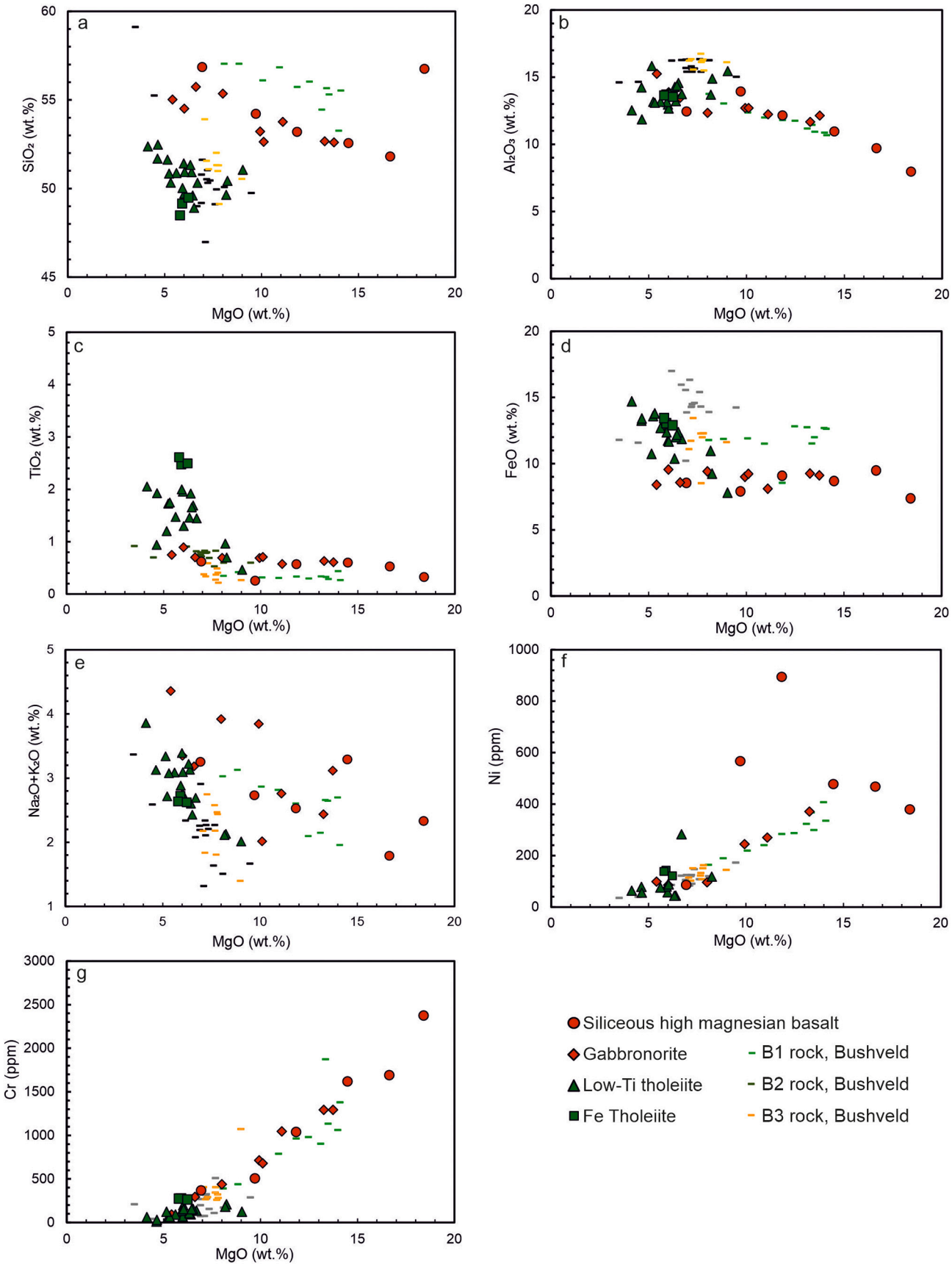

Fig. 6. Selected major element oxides plotted against MgO for the studied dykes.

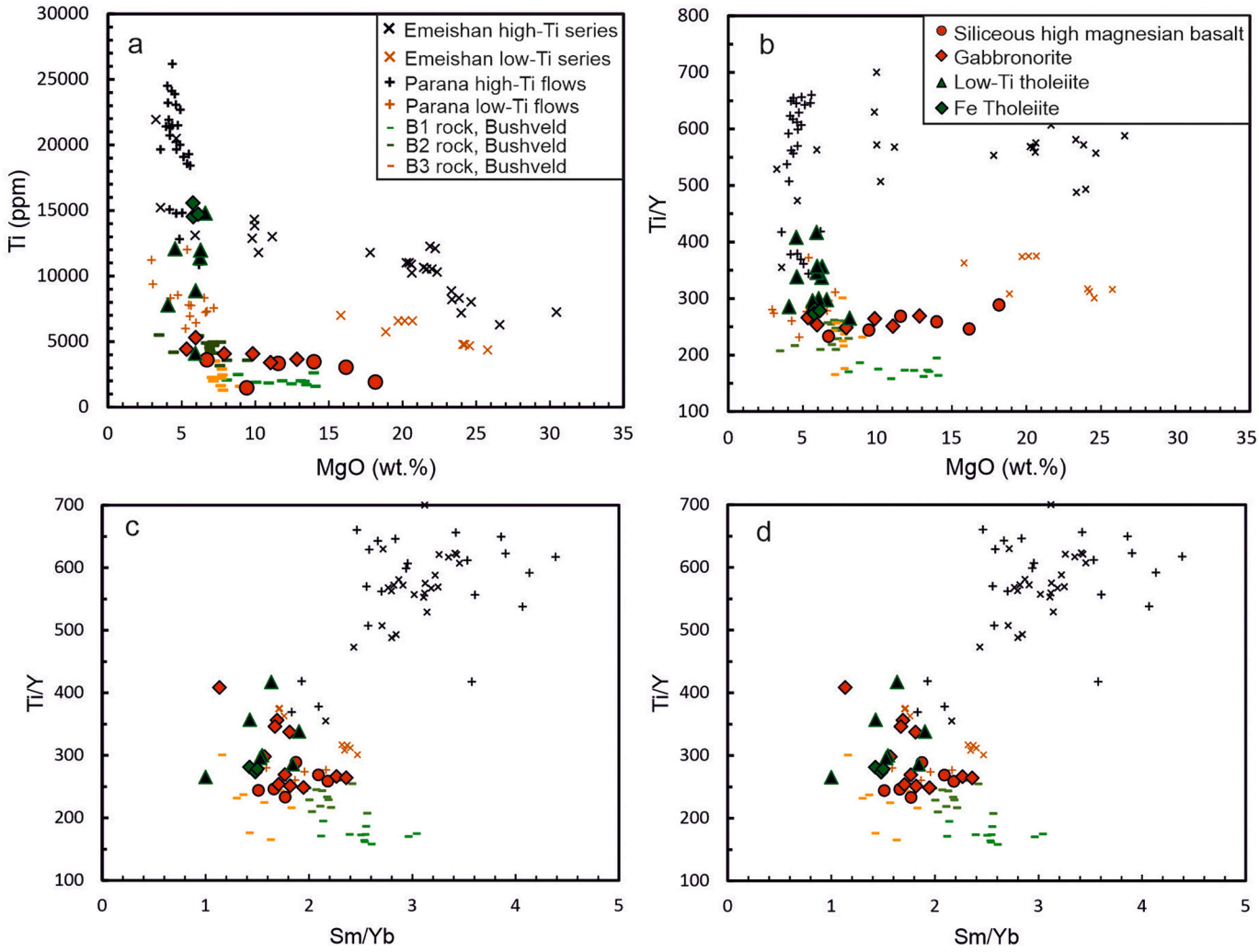

Fig. 7. Binary plots of MgO (wt%) vs Ti (ppm), MgO (wt%) vs. Ti/Y, Sm/Yb vs. Ti/Y, La/Yb vs. Ti/Y for our studies samples, high-Ti and Low-Ti basalts from the Paraná Magma Provice (Mansur et al., 2021) and the Emeishan Large Igneous Province (Arguin et al., 2016). Bushveld data are taken from Barnes et al. (2010).

with a minor amount of crustal contamination. Assuming a similar parental magma and crustal contaminant as in the case of the SHMB and GBNO dykes, the two-component mixing model indicates <3 wt% crustal contamination (Fig. 9). The obtained extent of crustal contamination is lower than the estimation of Puchtel et al. (1996) for the Vetreny belt komatiites, but it should be kept in mind that the selection of end-members of both ultramafic magma and crustal contaminants will result in considerable uncertainties. In addition, two component mixing may be too simplified if compared with the real assimilation fractionation contamination (AFC) processes. Later, we will present results of thermodynamic modelling of crustal contamination processes.

Another potential approach to constrain the mantle source to magmas is to consider PGE contents and ratios (Maier and Barnes, 2004). Relative to the primitive mantle with the estimated Pt about 7 ppb and Pd about 4 ppb (Maier and Barnes, 1999), the SCLM is generally depleted in Pt and Pd (by about 50–70%, about 5 ppb Pt, 2 ppb Pd) due to dissolution of most mantle sulphides during large degrees of melting that normally occur during the SCLM formation (Lorand and Luguet, 2016; Pearson et al., 2003). Metasomatic agents may increase the PGE content of the SCLM (Hughes et al., 2014), but the paucity of mantle samples that contain significantly higher Pt and Pd than primitive mantle (PM) suggests that most metasomatic agents are poor in PGE. This idea is consistent with the low PGE contents in Karelian group-II kimberlites (mostly <1 ppb Pt and Pd; Maier et al., 2017). However, because kimberlites represent ultra-low degrees of mantle melting, it would be desirable to determine PGE in larger-degree SCLM melts (e.g., the Nuanetsi picrites of the Karoo LIP in South Africa). One sample analysed by Maier et al. (2003) shows a moderate PGE content (12 ppb Pt + Pd) at high Pt/Pd (~2) and low Pd/Ir (~4), consistent with PGE depletion in the SCLM. All the dyke groups studied in the present project show relatively high PPGE contents and high Pd/Ir and Pd/Pt ratios, thus not supporting derivation from a SCLM source.

Maier et al. (2016) produced a number of MELTS (Ghiorso and Sack, 1995) models to constrain the mantle source of the Bushveld magmas. They simulated melting of the Kaapvaal SCLM by using mantle xenoliths hosted by Kaapvaal kimberlites. The resulting model melts were much lower in SiO_2 (~45 wt%) and higher in K_2O (~2.6 wt%) than the Bushveld SHMB magmas that are normally considered to be parental magma to the lower portions of the Bushveld Complex. Based on these results, the authors concluded that the Bushveld magmas are derived from the sub-lithospheric mantle. Yang et al. (2016) found that chromites from the most primitive magma in the Kemi and Monchepluton intrusions show chondritic Os isotope compositions, which is inconsistent with a SCLM derivation, as the latter generally has sub-chondritic $^{187}Os/^{188}Os$ (Peltonen and Brügmann, 2006; Shirey and Walker, 2003).

5.2. *Computer simulations of magma evolution*

The relationship between the relatively MgO-rich SHMB and GBNO dykes and the relatively MgO-poor tholeiitic dykes (LTTH and FTH)

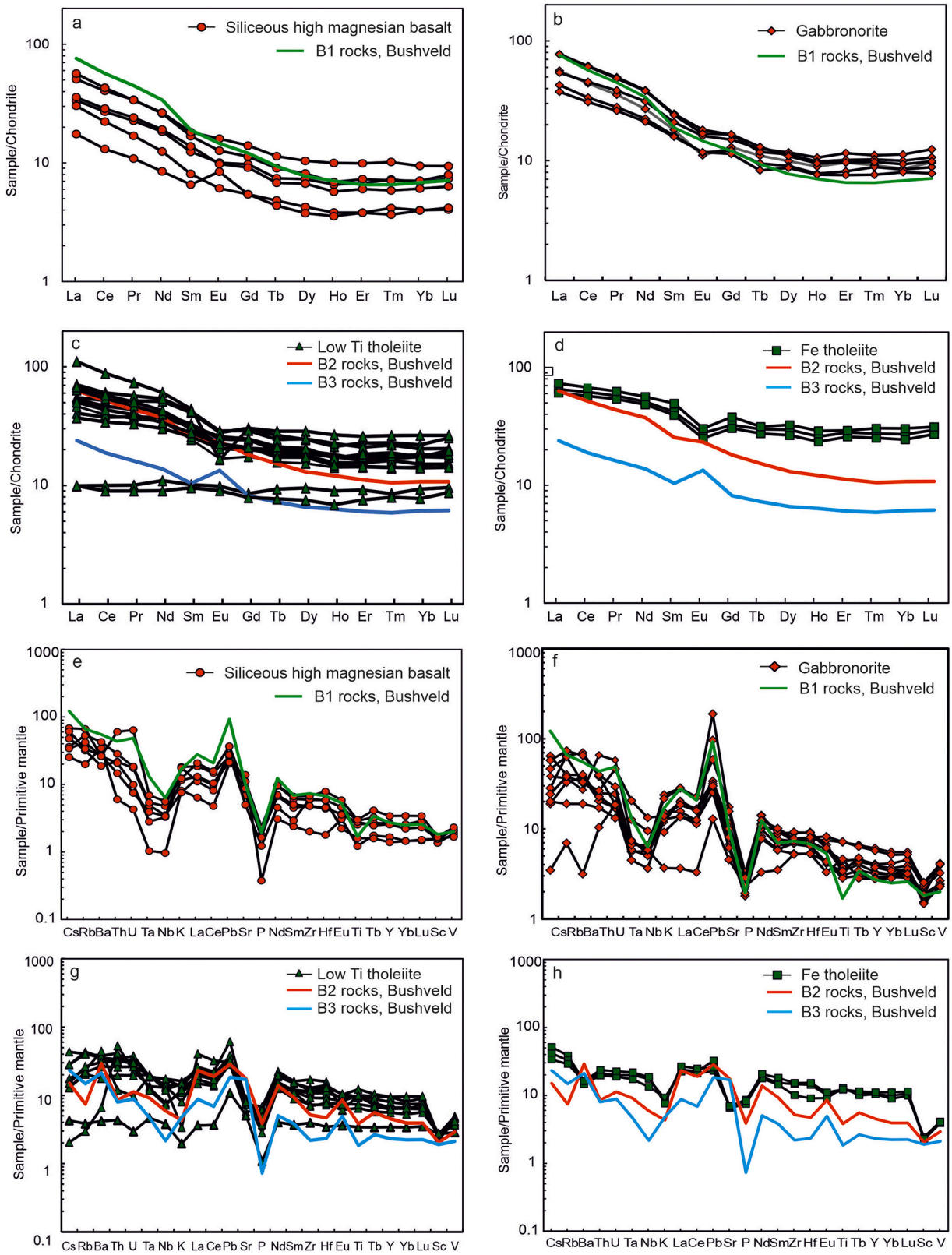

Fig. 8. Chondrite-normalised rare earth element (REE) patterns and primitive mantle-normalised lithophile trace element patterns for different dyke groups. Bushveld data are taken from Barnes et al. (2010) and normalisation values from Sun and McDonough (1989) and McDonough and Sun (1995).

remains enigmatic. It is interesting to note that other LIPs and layered intrusions also contain both SHMB and tholeiitic magma suites (Fig. 14) (e.g., Belomorian belt in Russia, Lobach-Zhuchenko et al., 1998; the Bushveld magmatic event on the Kaapvaal craton of South Africa, B1 and B2/B3 magmas, Sharpe et al., 1981; Barnes et al., 2010; the Stillwater Complex in Montana, Helz, 1995). The variation in the major element compositions of the Karelian SHMB and GBNO dykes is similar to that of SHMB dykes in the Belomorian belt and the Vetreny

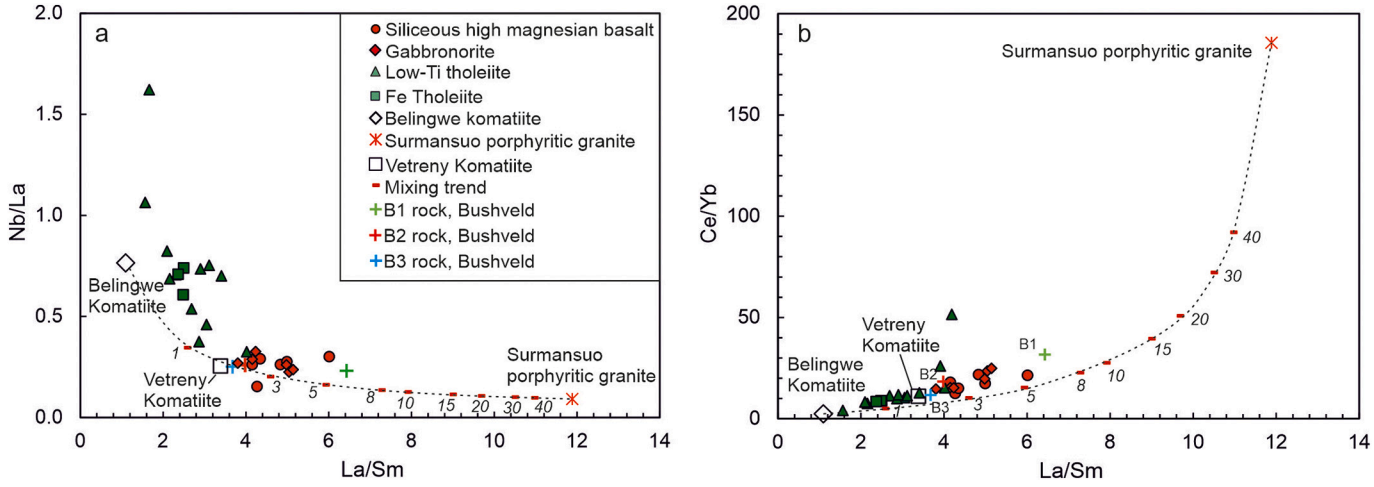

Fig. 9. Trace element ratios in the studied dykes showing a negative correlation between Nb/Th and La/Sm and a positive correlation between Ce/Yb and La/Sm. Simplified two component mixing calculation using komatiite and trondhjemite as end-members indicates <10% contamination for the tholeiite group and 5–20% for SHMB and GBNO. Primitive mantle values are from McDonough and Sun (1995). Comparative data for komatiite from Belingwe are from Shimizu et al. (2005), Vetreny komatiite from Puchtel et al. (1997), and Archaean trondhjemite from Mikkola et al. (2011).

Table 3
Chalcophile elements composition of different types of 2.45 Ga mafic dykes in Finland.

Sample No.	Rock	MgO	Ni	Os	Ir	Ru	Rh	Pt	Pd	Au	Cu
		wt%	ppm	ppb	ppb	ppb	ppb	ppb	ppb	ppb	ppm
K450–2	SHMB	14.0	403.7	0.4	0.8	2.8	1.2	8.5	7.2	–	85.3
K480	SHMB	11.6	890.1	0.4	0.6	2.4	0.8	5.6	8.9	0.9	76.4
O16	SHMB	6.7	81.8	0.1	0.3	0.7	1.3	12.0	11.9	1.8	85.4
R658	SHMB	9.4	552.3	0.3	0.8	1.2	2.8	9.0	1.8	–	27.7
13.4 SUO-93	SHMB	16.2	441.7	0.5	0.8	3.7	1.7	9.7	10.7	1.7	87.1
13.9.3-SUO-93	SHMB	18.2	369.6	0.4	0.9	5.8	3.5	8.4	4.4	0.8	39.2
AD31–1	GBNO	6.0	90.3	0.1	0.3	1.2	2.4	12.1	11.8	1.1	111.0
35 VEN-94	GBNO	7.9	98.6	–	0.1	0.9	1.6	7.9	8.6	2.2	59.8
4.4 VEN-93	GBNO	5.3	100.5	–	0.1	0.2	0.3	2.6	2.7	–	87.6
AD5–1	GBNO	12.8	368.4	0.1	0.4	2.4	1.5	14.0	16.0	0.9	91.4
AD5–2	GBNO	9.8	256.4	0.2	0.4	2.2	1.6	5.2	5.0	–	114.7
AD54–1	GBNO	11.0	248.1	0.2	0.5	2.8	2.8	21.1	22.0	2.4	88.0
AD12–1	GBNO	6.5	75.7	–	–	0.1	–	9.0	4.6	–	93.6
AD22–2	GBNO	10.0	152.2	0.1	0.5	–	–	17.0	–	1.7	105.2
AD37	GBNO	13.1	372.7	0.7	0.7	1.9	0.7	8.6	4.1	–	34.3
K395	LTTH	4.6	83.6	0.1	0.0	0.2	0.7	0.3	–	–	27.8
7.2. SUO-93	LTTH	6.6	278.7	0.1	0.1	0.3	0.4	2.1	2.8	1.0	142.6
AD14–3	LTTH	5.9	55.8	–	0.0	–	0.2	–	–	–	71.9
AD14–4	LTTH	6.3	45.9	0.1	–	0.4	0.9	–	–	–	75.5
AD27–1	LTTH	6.3	49.7	–	–	0.2	0.1	0.1	–	–	94.4
AD1–3	LTTH	5.9	80.3	–	–	–	–	0.7	–	–	141.7
AD2–1	LTTH	4.6	58.6	–	–	–	–	9.5	24.0	3.9	203.3
UD4	LTTH	6.1	90.6	–	–	–	–	2.9	–	–	100.3
UD7	LTTH	5.6	80.4	–	–	–	–	3.4	–	–	98.5
2-TD-93	LTTH	4.1	73.2	–	0.0	0.2	0.1	0.3	–	–	88.9
K477–4	LTTH	8.1	126.7	–	0.1	–	–	5.5	–	1.8	79.3
38-VEN-94	LTTH	6.0	88.1	–	–	–	–	11.0	22.3	–	240.3
AD1–1	LTTH	6.4	69.6	–	–	–	–	0.7	–	–	164.7
AD1–2	LTTH	6.3	68.3	–	–	–	–	1.0	–	–	161.0
AD3–2	LTTH	5.2	48.9	–	–	–	–	21.0	24.3	7.7	264.9
AD8–6	LTTH	5.2	48.6	–	–	–	–	18.6	–	6.2	281.0
1-UD-93	LTTH	5.2	68.9	–	–	–	–	3.3	–	–	120.3
AD60–1	LTTH	9.0	102.9	0.1	0.2	–	–	18.0	22.2	2.5	105.9
AD43–1	LTTH	8.0	107.1	0.2	0.2	–	0.5	19.8	21.9	1.5	160.4
WD-12	FTH	5.8	156.9	–	0.1	0.6	1.3	11.0	12.6	3.1	312.7
WD13	FTH	6.1	140.4	–	0.1	0.7	1.0	13.5	14.2	1.7	342.2
WD-14	FTH	5.8	132.5	0.1	0.1	0.7	1.1	12.2	14.0	1.9	281.4

komatiites, whereas the Karelian tholeiite dykes display similar variation as the tholeiites in the Kola and Belomorian belts (Fig. 14). One possibility is that the two contrasting magma types were derived from a common mantle plume source, but the SHMB/GBNO group experienced a higher degree of crustal contamination than the tholeiitic group. The contamination elevated the SiO_2 and alkali contents and considerably influenced the isotope and incompatible trace element ratios of the SHMB/GBNO group (Fig. 9). To test this hypothesis, we conducted thermodynamically constrained major element modelling using the recently published Magma Chamber Simulator (MCS) software (Bohrson

Table 4
Range of concentrations, average compositions, and standard deviations of PGE for each mafic dyke group.

Element	SHMB (n = 6)			GBNO (n = 9)			LTTH (n = 19)			FTH (n = 3)		
	Range	Aver.	STD	Range	Aver.	STD	Range	Aver.	STD	Range	Aver.	STD
Os	0.10–0.47	0.36	0.14	0.03–0.71	0.16	0.21	0.03–0.16	0.05	0.03	0.03–0.08	0.05	0.03
Ir	0.26–0.89	0.69	0.23	0.01–0.66	0.32	0.23	0.01–0.19	0.04	0.05	0.12–0.14	0.13	0.01
Ru	0.69–5.84	2.77	1.85	0.06–2.84	1.31	1.07	0.06–0.33	0.12	0.09	0.63–0.72	0.68	0.04
Rh	0.79–3.48	1.87	1.04	0.04–2.84	1.23	1.03	0.04–0.72	0.18	0.24	1–1.3	1.13	0.15
Pt	5.61–12.04	8.86	2.08	2.55–21.1	10.83	5.84	0.04–20.99	6.22	7.86	11.0–13.6	12.3	1.28
Pd	1.82–11.86	7.48	3.84	0.24–21.95	8.33	7.04	0.24–24.26	6.35	10.7	12.6–14.2	13.6	0.87
Au	0.24–1.83	0.94	0.68	0.24–2.41	1.03	0.88	0.24–7.66	1.45	2.30	1.72–3.15	2.24	0.78
Cu	30.9–94.4	68.6	26.3	66–116	92.7	18.53	22.4–254.4	121.6	58.1	289–341	321	27.9

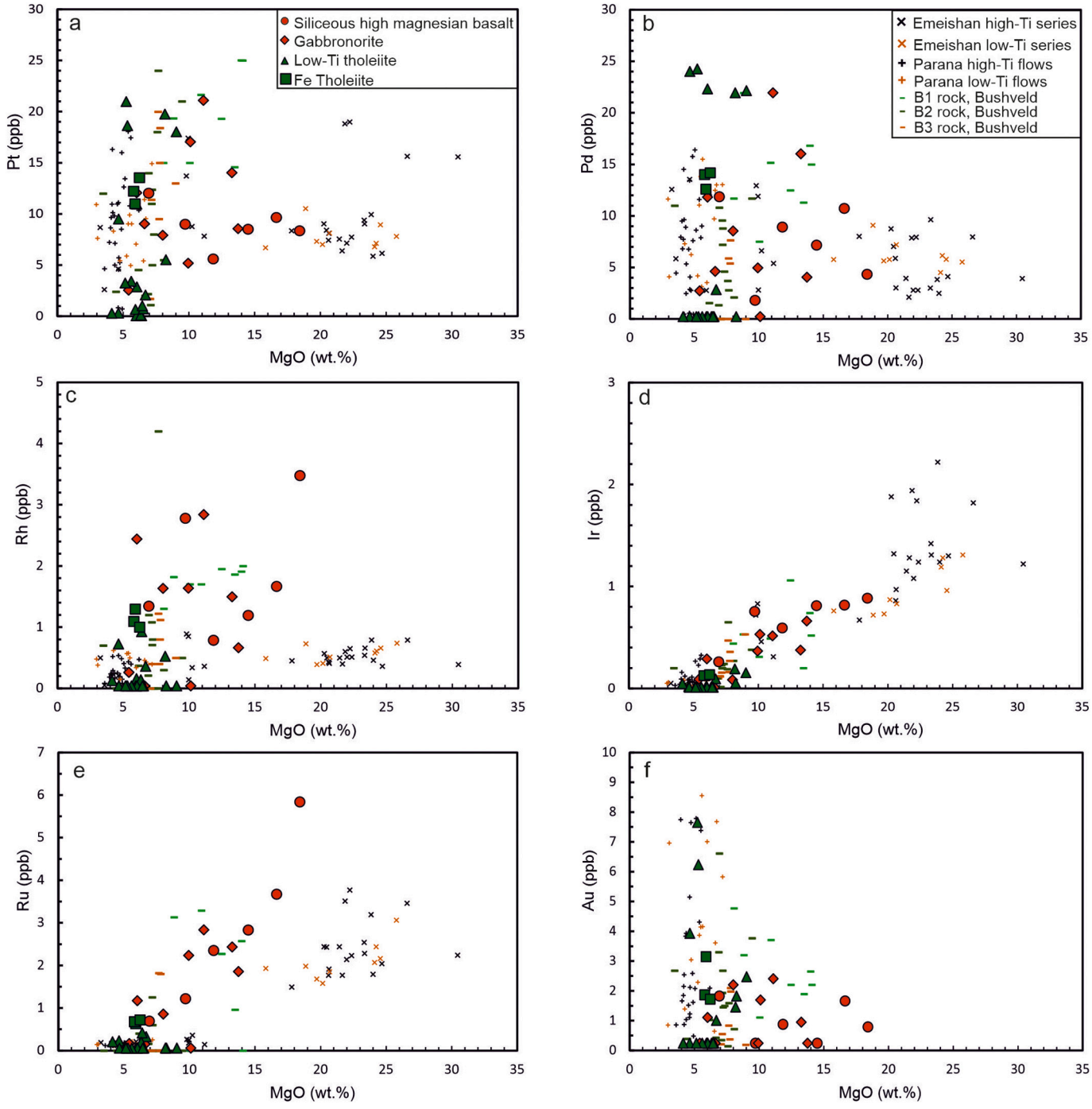

Fig. 10. Pt, Pd, Rh, Ru, Ir and Au vs. MgO diagrams for the studied dykes.

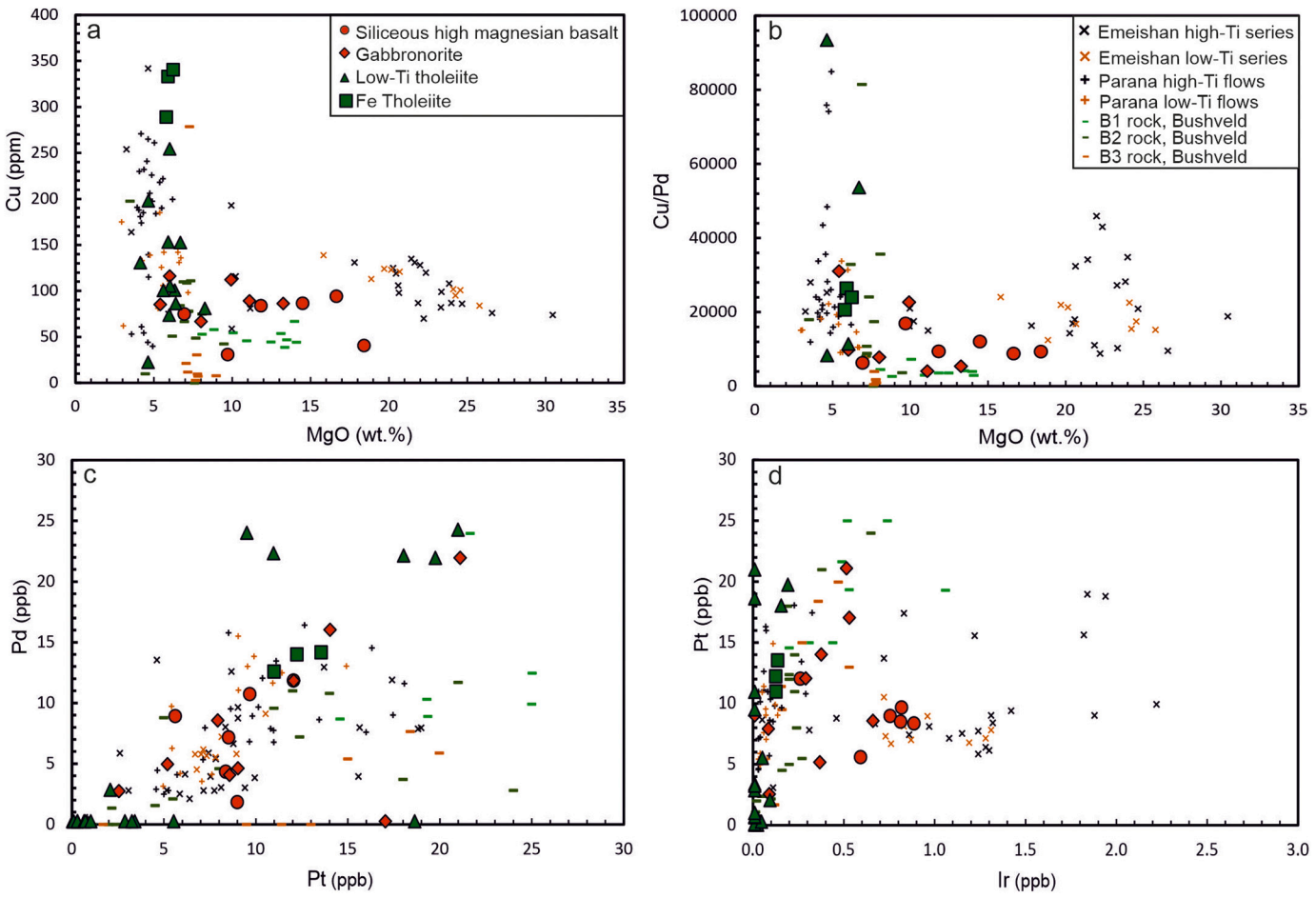

Fig. 11. Cu, Cu/Pd vs. MgO, Pd vs. Pt and Pt vs. Ir diagrams for the studied dykes.

et al., 2020). One crucial end-member needed in the modelling is an uncontaminated parental (initial) melt composition. The Vetreny belt komatiite likely is not a pristine mantle melt as it shows signs of crustal contamination (Puchtel et al., 1996). The Karelian tholeiitic dykes with their positive εNd (from −0.3 to +1.7) and low initial Sr (0.7022–0.7023) may in fact be less contaminated than the Vetreny komatiites, but most of them are relatively evolved and are thus unlikely to represent primary magmas. We thus chose an average composition of seven relatively primitive tholeiite dyke samples from the Karelian and Belomorian cratons and then added equilibrium liquidus olivine in 1 wt % steps until the calculated melt was in equilibrium with forsteritic mantle olivine (Fo_{92}). After adding 43 wt% of olivine, the melt reached a komatiitic composition with ~21 wt% MgO. We used this melt as the parental magma composition (Appendix A). The initial Fe oxidation state is assumed to be at $Fe^{2+}/Fe^{tot} = 0.88$ (Appendix A), but not forced through the runs, and the H_2O content is assumed to be 0.5 wt% based on the recent H_2O content estimation for Archaean komatiites by Sobolev et al. (2019). For the crustal contaminant, we chose a trondhjemite (A1906, Mikkola et al., 2011) from the Archaean Suomussalmi belt, a representative rock type for wall rocks of most Karelian mafic dykes and layered intrusions. In all the model calculations, the temperature steps were 5 °C. The assimilation-fractional crystallisation (AFC) model was conducted at a pressure of 300 MPa and the fractional crystallisation (FC) models were conducted at 100 MPa. Such conditions, where AFC takes place primarily at depth within a warm crust, and FC within a shallower cool crust, have been suggested for Phanerozoic LIPs (e.g., Heinonen et al., 2019). In the AFC model, the wall rock vs. parental melt ratio was 1:1 and the percolation threshold of the wall rock (i.e. the amount of melt that has to be generated before assimilation begins) was 10 wt% of melt (see Bohrson et al., 2020). In addition, to simulate early assimilation and pre-heating of the wall rock by previous magma pulses in an active rift environment, the initial temperature of the wall rock was set close to its solidus (690 °C at 300 MPa, see Heinonen et al., 2019). All output data are listed in the Electronic Appendix A.

To test whether the tholeiite dykes could be generated by fractionation of the calculated komatiitic parental magma, we simulated fractional crystallisation at 100 MPa. The modelled compositions generally replicate the compositional variation trend of the tholeiite dykes. This indicates that the komatiitic magma represents a reasonable end member in the modelling (Fig. 14). Some tholeiitic samples show slightly higher TiO_2 contents than the modelled trend (Figs. 14b, c). This could be a result of minor variations in the parental magma compositions. To generate the SHMB and GBNO dyke compositions, we simulated AFC at 300 MPa with the komatiitic magma as a starting composition. Due to residual plagioclase in the wall rock, the contaminated melt becomes depleted efficiently in Ca. The AFC model can produce the Vetreny parental liquid composition represented by chilled rocks with an MgO content of about 14.6 wt%, which corresponds to liquid compositions suggested for this magma type (Puchtel et al., 1996; Fig. 14). Continuous contamination yields a high SiO_2 content up to 62 wt% while MgO decreases to <4 wt%, slightly higher than the observed compositional variation in the SHMB and GBNO dykes. One possibility is that the AFC process that takes place in a warm crustal environment at depth is followed by fractional crystallisation within a colder crust at shallower levels (Heinonen et al., 2019, 2020). Hence, we simulated an FC model after 14 wt% crustal contamination at pressure conditions of 100 MPa. The major element compositions of the SHMB and GBNO dykes all plot

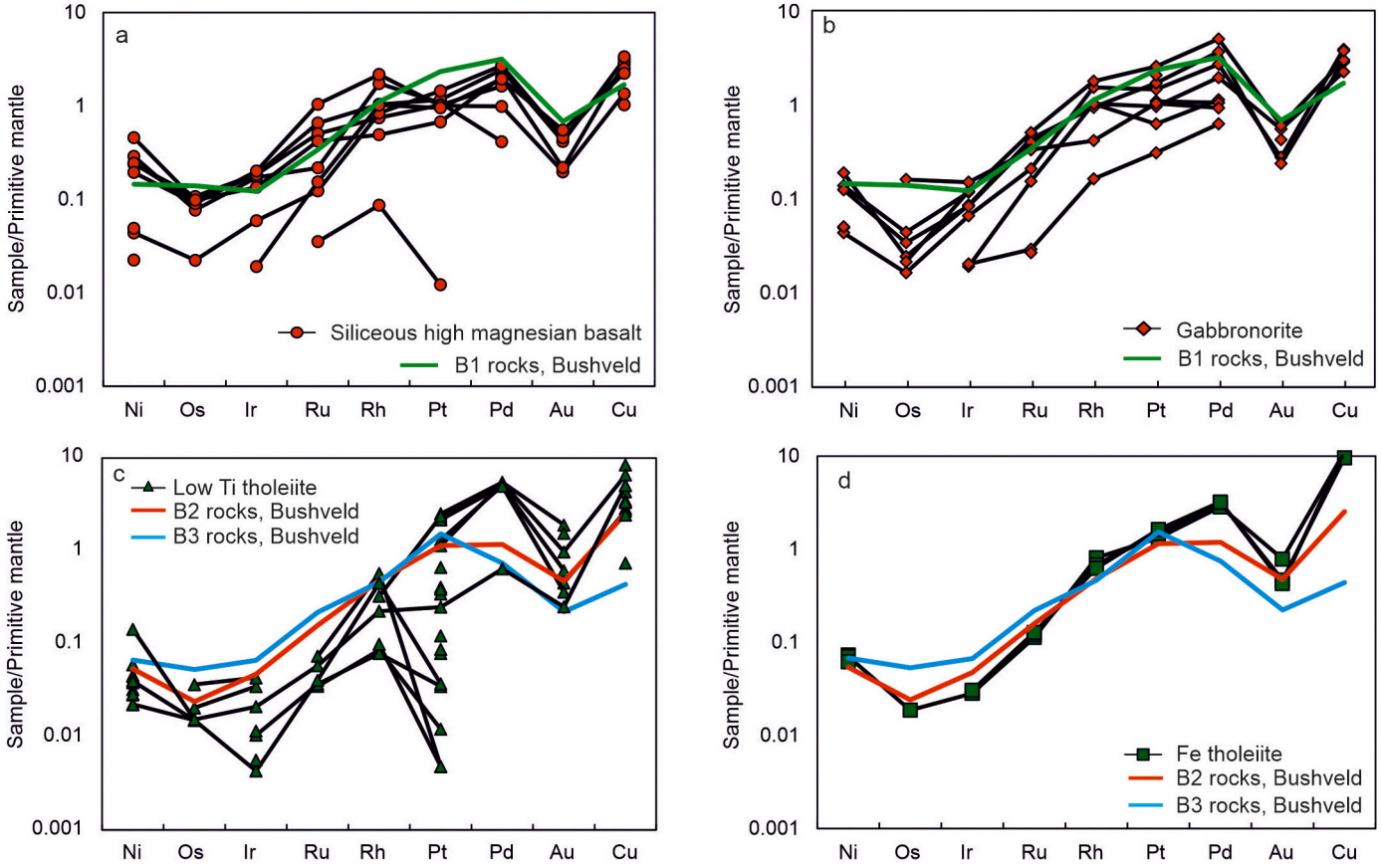

Fig. 12. Primitive mantle-normalised siderophile element patterns for the studied dykes. Normalisation values taken from (McDonough and Sun, 1995).

Table 5
In-situ Sr isotope composition of plagioclase from different types of 2.45 Ga mafic dykes in Finland.

Sample No.	Rock type	Grains (n)	$^{87}Rb/^{86}Sr$	Rb/Sr	$^{87}Sr/^{86}Sr_i$	2σ
9-SUO-92	SHMB	9	0.010	0.004	0.70303	0.00014
13.3-SUO-93	SHMB	9	0.005	0.002	0.70312	0.00016
13.7-SUO-93	SHMB	10	0.010	0.004	0.70323	0.00019
13.6-SUO-93	SHMB	13	0.005	0.002	0.70296	0.00030
7-SUO-93	SHMB	5	0.018	0.006	0.70398	0.00085
13.4-SUO-93	SHMB	8	0.005	0.002	0.70370	0.00069
14-SUO-93	GBNO	7	0.007	0.003	0.70324	0.00024
AD54–1-110	GBNO	10	0.006	0.002	0.70304	0.00038
AD22–3-110	GBNO	10	0.004	0.002	0.70376	0.00059
17-SUO-92	GBNO	6	0.018	0.006	0.70360	0.00030
AD54–6	GBNO	9	0.005	0.002	0.70313	0.00050
AD-22-2	GBNO	8	0.007	0.003	0.70319	0.00052
AD60–1	LTTH	6	0.013	0.005	0.70230	0.00021
1-TD-93	LTTH	9	0.012	0.004	0.70247	0.00030

between the AFC model and the FC model (Fig. 14), indicating that the chosen parameters are reasonable and a combined AFC and FC model can reproduce the compositions of the SHMB and GBNO dykes from a komatiitic parental melt (Fig. 14). In the modelling, the crystallisation order of komatiite is olivine-orthopyroxene-clinopyroxene-plagioclase-spinel, broadly consistent with the observed mineral assemblage observed in the Vetreny komatiite and the SHMB group dykes. The modelled most primitive olivine has Fo up to 92 mol%, slightly more primitive than the olivine in cumulates of the Vetreny komatiite with Fo up to 89 mol%, but comparable to that of the dunite unit in the Monchegorsk intrusion (Chistyakova et al., 2015; Puchtel et al., 1996). The

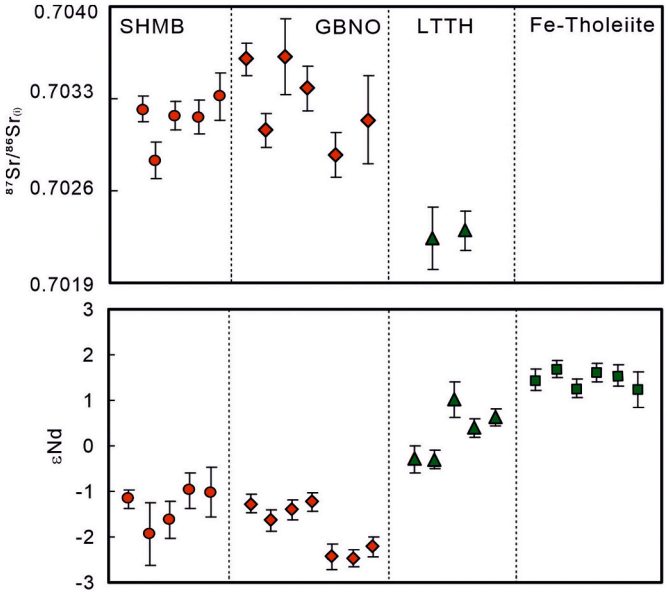

Fig. 13. In-situ Sr isotope compositions of plagioclase and bulk-rock Nd isotope compositions of the studied dykes. Nd isotope data taken from (Vuollo and Huhma, 2005).

modelled earliest liquidus orthopyroxene and clinopyroxene have Mg# of 85 and 84, respectively, comparable to the observed composition in both Vetreny komatiite (Puchtel et al., 1996), the SHMB dykes in this study (Fig. 5), and the Penikat intrusion (Alapieti and Halkoaho, 1995). Accordingly, the models are more compatible with a scenario where the

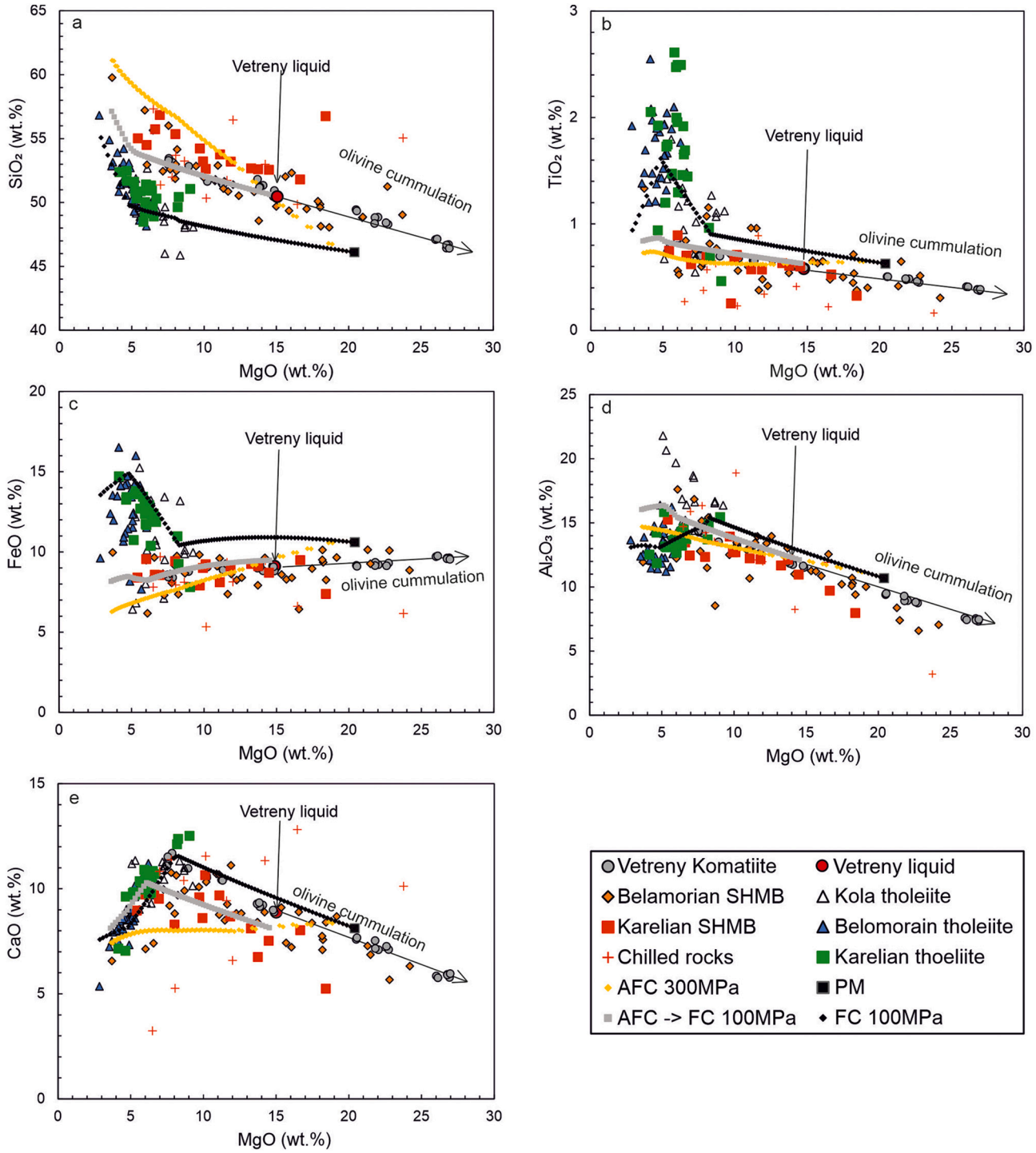

Fig. 14. MCS (Magma Chamber Simulator) major element modelling for different types of mafic dykes in Karelian, Belomorian and Kola regions at different pressures.

SHMB and GBNO dykes experienced an AFC process at a relatively deep crustal level (300 MPa), followed by a FC process in a shallower crust, whereas the LTTH and FTH dykes experienced mainly a FC process with a very low degree of crustal contamination (Figs. 14, 15a). On the other hand, a model that the SHMB suite magma derived from melting of SCLM and the tholeiitic suite magma from plume mantle (Fig. 15b) is not favoured.

As was stated above, the tholeiitic dykes all have relatively low MgO contents (<8 wt%). Similar observations have been made in the Belomorian, Kola and Superior cratons (Lobach-Zhuchenko et al., 1998; Vogel et al., 1998). It is possible that more primitive members have not been found, are not exposed, or were never emplaced in the shallow crust, but the similarity among different cratons renders it possible that primitive end-members for the tholeiitic suites do not exist. As a further note, the tholeiitic dykes show slightly higher TiO_2 contents than the SHMB and GBNO suites (Fig. 14b). This raises the possibility that, as an alternative model, the tholeiites may have formed by lower degrees of partial melting, at higher pressures in deeper mantle domains from a garnet peridotite mantle source (Fig. 15c). A similar model has been proposed to explain the genesis of a high-Ti magma suite in the

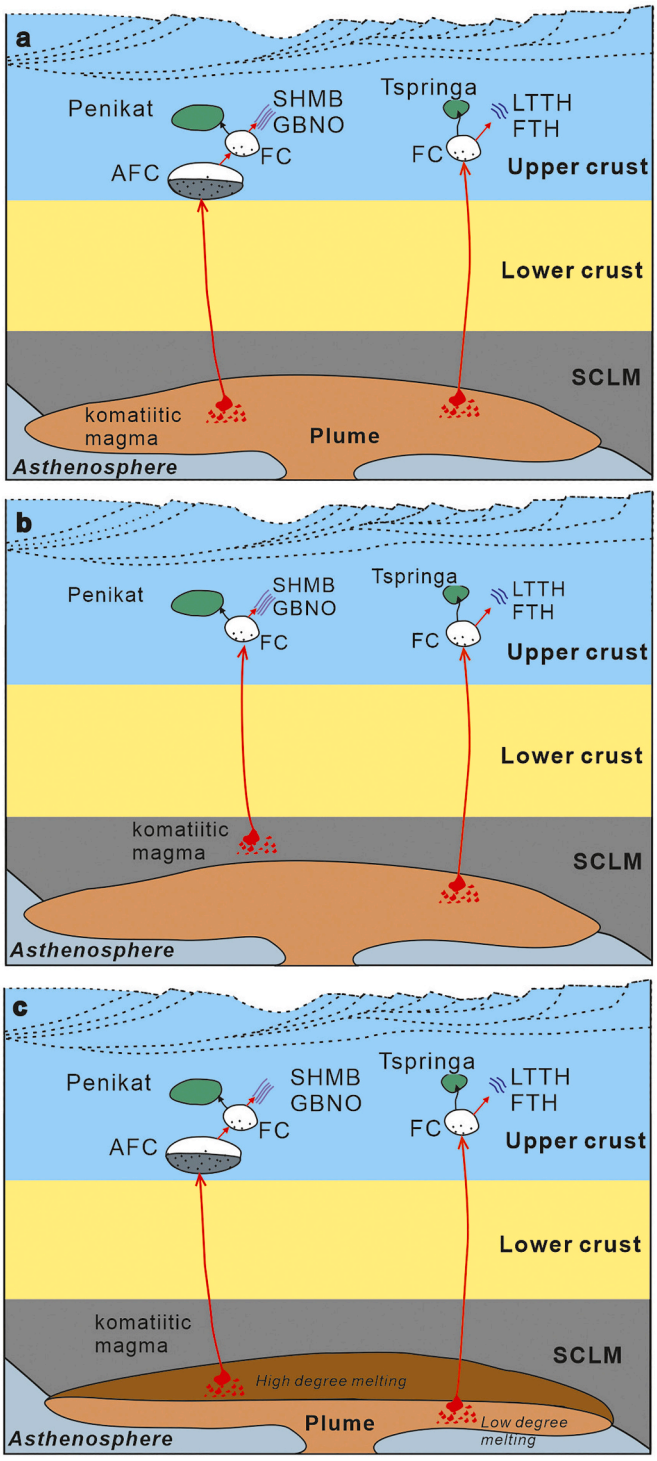

Fig. 15. Model of the petrogenesis of magmas of different dykes and correlation with coeval layered intrusions (not scaled). A. Common magma source for all dyke types, B. SHMB group dykes are derived from melting of SCLM and tholeiitic dykes from plume mantle, C. Dykes are generated at variable mantle levels.

Emeishan LIP (Wang et al., 2007). However, both the LLTH and FTH dykes in Fennoscandia show a similar Ti content to that of the low-Ti magma suite of Emeishan and Parana, but considerably lower Ti contents than the Emeishan and Paraná high-Ti magma suites (Figs. 6c, 7). The relative low Ti content is coupled with lower Sm/Yb than in the Emeishan and Paraná high-Ti magma series (Fig. 7c), indicating that the melting regime involved shallow spinel peridotite mantle and a relatively high degree of partial melting.

5.3. Relationship between dykes and layered intrusions

A genetic relationship between the dyke suites and the coeval and spatially associated layered intrusions has long been assumed, based mainly on Nd isotope evidence. Hanski et al. (2001) showed that many of the layered intrusions share negative εNd values with the SHMB and GBNO dykes. In contrast, the Tsipringa intrusion in the Olanga layered complex has positive εNd (+1), which is similar to the Nd isotope composition of the tholeiitic dykes studied here (Vuollo and Huhma, 2005). Maier et al. (2018) showed that the cumulates of the Penikat intrusion and the Loljunmaa feeder dyke have a similar Nd isotope and trace element signature to those of the SHMB and GBNO dykes. Similarly, the dykes in the vicinity of the Portimo complex show major element characteristics similar to the SHMB and GBNO dykes (Iljina, 1994). In the case of the Kemi intrusion, there are neither coeval dykes nor chilled margins. Nevertheless, the relatively radiogenic initial Sr isotope composition (0.7027) suggests a magma composition similar to the SHMB dykes (Yang et al., 2016). The Sr isotope data obtained for the SHMB and GBNO dykes in the present study resemble those of the Burakovka Complex in south-eastern Karelia and the Kemi intrusion, consistent with the concept that these dykes crystallised from parental magmas similar to those which produced the layered intrusions (Amelin and Semenov, 1996; Yang et al., 2016).

One common feature of many Fennoscandian 2.45 Ga layered intrusions, including the intrusions of the Tornio-Näränkävaara belt, is that the upper parts tend to have a much lower Cr content than the lower portions (Alapieti and Halkoaho, 1995; Halkoaho et al., 1990; Iljina, 1994; Maier et al., 2018). Based on mineralogical and bulk-rock geochemical data, it has been suggested two parental magma types, one high in Cr (>1000 ppm) and the other low in Cr (<600 ppm), have been involved in these intrusions (Alapieti et al., 1990; Vogel et al., 1998). The authors argue that the high-Cr magma has a similar composition to the SHMB dykes, with elevated SiO_2 content and fractionated REE patterns, whereas the low-Cr magma, featuring less fractionated REE patterns, is related to the tholeiitic dykes. A similar pattern of coexisting SHMB and tholeiitic magmas has been observed in the Bushveld Complex. The rocks of the Lower and Lower Critical Zones of the intrusion are relatively rich in Cr and share an SHMB signature with a suite of pyroxenitic sills in the floor of the complex (termed B1 sills suite by Sharpe et al., 1981). The rocks of the Main and Upper Zones are relatively poor in Cr and share a tholeiitic signature with fine-grained gabbronoritic footwall sills (B2 and B3 sill suites). The Critical Zone, hosting the Merensky Reef and UG2 chromitite, has a hybrid SHMB–tholeiitic composition (Karykowski et al., 2017; Kruger, 1994; Sharpe et al., 1981; Yang et al., 2019).

Regarding to the relationship between the tholeiitic dykes and the Fennoscandian intrusions, the dykes have positive initial εNd values, which are distinct from the negative initial εNd values of the upper part of the Penikat, Koitelainen and Akanvaara intrusions (εNd = −1.3 -2.4, Hanski et al., 2001; Maier et al., 2018). Also, plagioclase grains from the tholeiitic dykes show low initial $^{87}Sr/^{88}Sr$ of ~0.7024 (Fig. 13), clearly lower than plagioclase from the Penikat intrusion (0.7027–0.7032) (Rivas, 2022), which are more consistent with the initial $^{87}Sr/^{88}Sr$ ratios of the SHMB and GBNO dykes (0.7030–0.7037, Fig. 13). Maier et al. (2018) proposed that the upper part of the Penikat intrusion may have been derived from an evolved SHMB magma that ascended from a deeper staging magma chamber, and had a low Cr content due to extensive crystal fractionation. This model is consistent with our new compositional data of clinopyroxene showing that some of the SHMB dykes had relatively low Cr and MgO contents. Specifically, clinopyroxene from the Penikat intrusion plot in the same trend defined by the SHMB and GBNO dykes in terms of Mg#, TiO_2, MnO, and Cr_2O_3 (Fig. 5).

The PELE modelling (Boudreau, 1999) carried out by Maier et al. (2018) suggests that the magma parental to the Penikat intrusion was

more evolved than the average SHMB composition. Possibly the dykes could have accumulated some Mg-rich minerals (olivine, orthopyroxene), or the magma parental to the Penikat intrusion experienced some fractionation before its final emplacement.

5.4. Sulphide saturation history and implications for PGE exploration

To form a PGE-rich sulphide deposit, it is critical that the magma remains sulphur undersaturated during its ascent through the crust or no sulphide liquid settles out of the magma. The SHMB and GBNO samples have PGE-undepleted mantle-normalised siderophile element patterns (Figs. 12a, b), with Pd contents up to 22 ppb and mantle-like Cu/Pd and Cu/Zr ratios (Fig. 11b), indicating that the magma was sulphur undersaturated during high-degree partial melting of the mantle and remained so *en route* to the upper crust. This renders the magmas prospective to form PGE deposits (e.g., Naldrett, 2004). However, one SHMB sample and two GBNO samples with a relatively low MgO content (~7 wt%) show low PGE concentrations (Pt <0.31 ppb). In addition, there is a decrease in both the Cu content and Cu/Zr ratio in the more evolved magmas (MgO, 5–10 wt%) (Fig. 11a), suggesting that these relatively evolved magmas reached saturation in sulphide melt. Notably, PGE reefs occur in both relatively primitive and relatively differentiated portions of the 2.45 Ga layered intrusions (e.g., Penikat, Portimo, Koillisma) (Maier et al., 2018), but the latter tend to be richer in PGE.

Regarding the tholeiitic dykes, the most primitive samples (LTTH) have broadly mantle-like Cu/Pd ratios (Fig. 11b) indicating that the magmas did not reach sulphide saturation during the early stage of their differentiation. Some of the LTTH samples show high Pd contents ranging from 20 to 24 ppb, which are close to the highest values reported for basaltic rocks worldwide (Fiorentini et al., 2010). The high PGE contents of these samples are unlikely a result from re-mobilisation of metals during low-T alteration as they also show the highest Pt contents of 10–20 ppb (Fig. 11c). Instead, one could suggest that the high PGE contents of the tholeiites were generated through fractionation of a more primitive magma. The problem with this model is that some studies have shown Pt to be compatible during fractionation of sulphide-undersaturated silicate melt at certain oxygen fugacity (e.g., Park et al., 2013). This would result in relatively high Pd/Pt ratios, consistent with the elevated Pd/Pt in the upper portions of many layered intrusions (e.g., Bushveld, Maier et al., 2013).

In the more differentiated members of the tholeiitic dyke suite (MgO = 4–6 wt%), PGE and Cu show large variation, with Pt and Pd contents ranging from <1 ppb to 20 ppb, indicating that sulphide melt saturation was reached during an advanced stage of fractionation. Interestingly, the FTH dykes are strongly enriched in Cu (400 ppm) at moderate Pt and Pd contents of around 10–14 ppb. The Cu/Pd ratio ranges from 20,000 to 26,000, being significantly higher than that in PM, but it is difficult to explain the high Cu/Pd ratio by a model of sulphide melt segregation as this should have caused a strong PGE depletion. Possibly, FTH dykes assimilated a small amount of Cu- and PGE-rich sulphide melt during their crustal ascent. However, these samples contain moderate amounts of PGE (12–14 ppb Pd) without significant enrichment. The other option is that high Cu is a consequence of enrichment due to metasomatic fluids (Le Vaillant et al., 2016), which is supported by the relatively high degree of alteration of these samples.

From the above discussion, it appears that all magma types occurring in the 2.45 Ga dyke suites are fertile in terms of PGE at a relatively unevolved stage. Depletion in PGE is restricted to some of the most evolved samples, suggesting that sulphide melt saturation was reached during advanced fractionation, which is commonly observed in flood basalt provinces. In the SHMB suite, sulphide melt saturation occurred at a slightly earlier stage (7–8% MgO) than in the tholeiitic suites (5 wt% MgO), possibly because the former underwent more crustal contamination. The obtained data on these 2.45 Ga dyke suites suggest that all stratigraphic levels of the coeval layered intrusions have potential to host PGE mineralisation.

6. Conclusions

The ~2.45 Ga dykes in northern and eastern Finland and adjacent parts of Russian Karelia, which are coeval with the PGE-mineralised layered intrusions, comprise several compositionally distinct types, including siliceous high-magnesian basalt, gabbronorite, low-Ti tholeiite and Fe-rich tholeiite dykes.

- The SHMB group dykes were likely derived via AFC from a komatiitic melt, followed by FC at a relatively low pressure, whereas the tholeiitic dykes represent less contaminated magmas generated dominantly by crystal fractionation. Alternatively, the SHMB dykes may have been derived from a SCLM mantle whereas the tholetiite dykes from a plume mantle, or the two types of dykes derived from different part of a mantle plume with different meting degree, though these latter two models are not favoured in this study.
- The lower portions of most of the Finnish PGE-mineralised intrusions (e.g., Penikat, Portimo) appear to have crystallised from a primitive SHMB-like magma with high MgO and Cr contents, whereas the upper portions of the intrusions were crystallised from a fractionated SHMB magma with lower MgO and Cr contents. The parental magma of the Tsipringa intrusion has a tholeiitic affinity. There is currently no clear evidence to suggest that individual layered intrusions crystallised from hybrid SHMB-tholeiitic magmas.
- Most of the mafic dykes are undersaturated in sulphides and fertile in PGE, but several of the most differentiated samples have evidently reached sulphide saturation, indicating a high potential for PGE deposits.

Funding

This work was co-funded by the K.H. Renlund Foundation, European Union and UK Research and Innovation (SEMACRET, 101057741), Korlactic CBC, Academy of Finland for J.S. Heinonen (Grant no. 295129) and a scholarship from the Finnish Graduate School of Geology to F.-F. Guo.

Declaration of Competing Interest

The authors declare that they have no known competing financial interests or personal relationships that could have appeared to influence the work reported in this paper.

Acknowledgements

We thank the very careful and helpful suggestions by Dr. Tuomo Karinen and an anonymous reviewer, and the efficient handling of co-editor-in chief Dr. Greg Shellnut. Sari Forss is thanked for preparing thin sections and Kari Moisio is thanked for help with ArcGIS software.

Appendix A. Supplementary data

Supplementary data to this article can be found online at https://doi.org/10.1016/j.lithos.2023.107206.

References

Alapieti, T.T., Halkoaho, T.A.A., 1995. Cryptic variation of augite in the Penikat Layered Intrusion, Northern Finland, with reference to megacyclic units and PGE-enriched zones. Mineral. Petrol. 54, 11–24.

Alapieti, T.T., Filén, B.A., Lahtinen, J.J., Lavrov, M.M., Smolkin, V.F., Voitsekhovsky, S. N., 1990. Early proterozoic layered intrusions in the northeastern part of the Fennoscandian Shield. Mineral. Petrol. 42, 1–22.

Amelin, Y.V., Semenov, V.S., 1996. Nd and Sr isotopic geochemistry of mafic layered intrusions in the eastern Baltic shield: Implications for the evolution of Paleoproterozoic continental mafic magmas. Contrib. Mineral. Petrol. 124, 255–272.

Amelin, Y.V., Heaman, L.M., Semenov, V.S., 1995. U-Pb geochronology of layered intrusions in the eastern Baltic Shield: implications for the timing and duration of Paleoproterozoic continental rifting. Precambrian Res. 75, 31–46.
Arguin, J.P., Pagé, P., Barnes, S.J., Yu, S.Y., Song, X.Y., 2016. The effect of chromite crystallization on the distribution of osmium, iridium, ruthenium and rhodium in picritic magmas: an example from the Emeishan large Igneous province, Southwestern China. J. Petrol. 57, 1019–1048.
Arndt, N., 2013. The Lithospheric mantle plays no active role in the formation of orthomagmatic ore deposits. Econ. Geol. 108, 1953–1970.
Barnes, S.J., Maier, W.D., Curl, E.A., 2010. Composition of the marginal rocks and sills of the Rustenburg layered suite, Bushveld complex, South Africa: implications for the formation of the platinum-group element deposits. Econ. Geol. 105, 1491–1511.
Bayanova, T., Korchagin, A., Mitrofanov, A., Sero, V.P., Ekimova, N., Nitkina, E., Kamensky, I., Elizarov, D., Huber, M., 2019. Long-lived mantle plume and polyphase evolution of Palaeoproterozoic PGE intusions in the Fennoscandian Shield. Minerals 9, 59.
Bohrson, W.A., Spera, F.J., Heinonen, J.S., Brown, G.A., Scruggs, M.A., Adams, J., Takach, M.K., Zeff, G., Suikkanen, E., 2020. Diagnosing open-system magmatic processes using the Magma Chamber Simulator (MCS): Part I—major elements and phase equilibria. Contrib. Mineral. Petrol. 175.
Boudreau, A.E., 1999. PELE—a version of the MELTS software program for the PC platform. Comput. Geosci. 201–203.
Chistyakova, S., Latypov, R., Zaccarini, F., 2015. Chromitite dykes in the Monchegorsk layered intrusion, Russia: in situ crystallization from chromite-saturated magma flowing in conduits. J. Petrol. 56, 2395–2424.
Ernst, R., Bleeker, W., 2010. Large igneous provinces (LIPs), giant dyke swarms, and mantle plumes: significance for breakup events within Canada and adjacent regions from 2.5 Ga to the present. Can. J. Earth Sci. 47, 695–739.
European Commission, 2020. Communication from the Commission to the European Parliament, the Council, the European Economic and Social Committee and the Commttee of the Regions 10–27.
Fiorentini, M.L., Barnes, S.J., Lesher, C.M., Heggie, G.J., Keays, R.R., Burnham, O.M., 2010. Platinum group element geochemistry of mineralized and nonmineralized komatiites and basalts. Econ. Geol. 105, 795–823.
Ghiorso, M.S., Sack, R.O., 1995. Chemical mass transfer in magmatic processes. IV. A revised and internally consistent thermodynamic model for the interpolation and extrapolation of liquid-solid equilibria in magmatic systems at elevated temperatures and pressures. Contrib. Mineral. Petrol. 119, 197–212.
Halkoaho, T.A.A., Alapieti, T.T., Lahtinen, J.J., 1990. The Sompujärvi PGE reef in the Penikat layered intrusion, northern Finland. Mineral. Petrol. 42, 39–55.
Hanski, E., 2012. Evolution of the Palaeoproterozoic (2.50–1.95 Ga) non-orogenic magmatism in the eastern part of the Fennoscandian Shield. In: Melezhik, V.A., Prave, A.R., Hanski, E.J., Fallick, A.E., Lepland, A., Kump, L.R., Strauss, H. (Eds.), Reading the Archive of Earth's Oxygenation. Volume 1: the Palaeoproterozoic of Fennoscandia as Context for the Fennoscandian Arctic Russia – Drilling early Earth Project. Springer-Verlag, Berlin, Heidelberg, pp. 179–245.
Hanski, E., Walker, R.J., Huhma, H., Suominen, I., 2001. The Os and Nd isotopic systematics of c. 2.44 Ga Akanvaara and Koitelainen mafic layered intrusions in northern Finland. Precambrian Res. 109, 73–102.
Heinonen, J.S., Luttinen, A., Spera, F.J., Bohrson, W.A., 2019. Deep open storage and shallow closed transport system for a continental flood basalt sequence revealed with Magma Chamber Simulator. Contrib. Mineral. Petrol. 174, 87.
Heinonen, J.S., Bohrson, W.A., Spera, F.J., Brown, G.A., Scruggs, M.A., Adams, J., 2020. Diagnosing open-system magmatic processes using the Magma Chamber Simulator (MCS): part II—trace elements and isotopes. Contrib. Mineral. Petrol. 175, 1–21.
Helz, R.T., 1995. The Stillwater complex, Montana: a subvolcanic magma chamber? Am. Mineral. 80, 1343–1346.
Hickey, R.L., Frey, F.A., 1982. Geochemical characteristics of boninite series volcanics: implications for their source. Geochim. Cosmochim. Acta 46, 2099–2115.
Hölttä, P., Heilimo, E., Huhma, H., Juopperi, H., Kontinen, A., Konnunaho, J., Lauri, L., Mikkola, P., Paavola, J., Sorjonen-Ward, P., 2012. Archaean complexes of the Karelia Province in Finland. Geol. Surv. Finland Spec. Pap. 54, 9–20.
Hughes, H.S.R., McDonald, I., Goodenough, K.M., Ciborowski, T.J.R., Kerr, A.C., Davies, J.H.F.L., Selby, D., 2014. Enriched lithospheric mantle keel below the Scottish margin of the North Atlantic Craton: evidence from the Palaeoproterozoic Scourie Dyke Swarm and mantle xenoliths. Precambrian Res. 250, 97–126.
Huhma, H., Cliff, R.A., Perttunen, V., Sakko, M., 1990. Sm-Nd and Pb isotopic study of mafic rocks associated with early Proterozoic continental rifting: the Peröpohja schist belt in northern Finland. Contrib. Mineral. Petrol. 104, 369–379.
Huhma, H., Hanski, E., Kontinen, A., Vuollo, J., Mänttäri, I., Lahaye, Y., 2018. Sm–Nd and U–Pb Isotope Geochemistry of the Palaeoproterozoic Mafic Magmatism in Eastern and Northern Finland. Geological Survey of Finland, Geological Survey of Finland, Bulletin 405, 150 pages, 128 figures, 1 table and 11 appendice.
Huhtelin, T., 2015. The kemi chromite deposit. In: Maier, W.D., Lahtinen, R., O'Brien, H. (Eds.), Mineral Deposits of Finland. Elsevier, pp. 165–178.
Huppert, H.E., Sparks, R.S.J., 1989. Chilled margins in igneous rocks. Earth Planet. Sci. Lett. 92, 397–405.
Iljina, M., 1994. The Portimo Layered Igneous Complex: With Emphasis on Diverse Sulphide and Platinum-Group Element Deposits. Doctoral dissertation. University of Oulu.
Iljina, M., Alapieti, T., McElduff, B.M., 1992. Platinum-group element mineralization in the Suhanko-Konttijärvi intrusion, Finland. Aust. J. Earth Sci. 39, 303–313.
Iljina, M., Maier, W.D., Karinen, T., 2015. PGE-(Cu-Ni) deposits of the Tornio-Näränkävaara belt of intrusions (Portimo, Penikat, and Koillismaa). In: Maier, W.D., Lahtinen, R., O'Brien, H. (Eds.), Mineral Deposits of Finland. Elsevier, pp. 133–164.
Karinen, T., 2010. The Koillismaa Intrusion Northeastern Finland - Evidence for PGE Reef Forming Processes in the Layered Series. Geological Survey of Finland, Bulletin, p. 404.
Karinen, T., Hanski, E., Taipale, A., 2015. The mustavaara Fe-Ti-V oxide deposit. In: Maier, W.D., Lahtinen, R., O'Brien, H. (Eds.), Mineral Deposits of Finland. Elsevier, pp. 179–194.
Karinen, T., Moilainen, M., Kuva, Jukka, Lahaye, Y., Datar, B., Yang, S.H., 2022. Mustavaara Revisited: A Revised Genetic Model for Orthomagmatic Fe–Ti–V Mineralisation in the Koillismaa Intrusion. Geological Survey of Finland, Bulletin, p. 414.
Karykowski, B.T., Yang, S.H., Maier, W.D., Lahaye, Y., Lissenberg, C.J., O'Brien, H., 2017. In situ sr isotope compositions of plagioclase from a complete stratigraphic profile of the Bushveld complex, South Africa: evidence for extensive magma mixing and percolation. J. Petrol. 58, 2285–2308.
Karykowski, B.T., Maier, W.D., Groshev, N.Y., Barnes, S.J., Pripachkin, P., McDonald, I., 2018. Origin of reef-style PGE mineralization in the Paleoproterozoic Monchegorsk complex, Kola Region, Russia. Econ. Geol. 113, 1333–1358.
Kruger, F.J., 1994. The Sr-isotopic stratigraphy of the western Bushveld complex. S. Afr. J. Geol. 97, 393–398.
Le Vaillant, M., Barnes, S.J., Fiorentini, M.L., Santaguida, F., Törmänen, T., 2016. Effects of hydrous alteration on the distribution of base metals and platinum group elements within the Kevitsa magmatic nickel sulphide deposit. Ore Geol. Rev. 72, 128–148.
Lobach-Zhuchenko, S.B., Arestova, N.A., Chekulaev, V.P., Levsky, L.K., Bogomolov, E.S., Krylov, I.N., 1998. Geochemistry and petrology of 2.40-2.45 Ga magmatic rocks in the north-western Belomorian Belt, Fennoscandian Shield, Russia. Precambrian Res. 92, 223–250.
Lorand, J.-P., Luguet, A., 2016. Chalcophile and siderophile elements in mantle rocks: Trace elements controlled by trace minerals. Rev. Mineral. Geochem. 81, 441–488.
Maier, W.D., Barnes, S.J., 1999. Platinum-group elements in silicate rocks of the lower, critical, and main zones of the Bushveld complex. J. Petrol. 40, 1647–1671.
Maier, W.D., Barnes, S.J., 2004. Pt/Pd and Pd/Ir ratios in mantle-derived magmas: a possible role for mantle metasomatism. S. Afr. J. Geol. 107, 333–340.
Maier, W.D., Hanski, E.J., 2017. Layered mafic-ultramafic intrusions of Fennoscandia: Europe's treasure chest of magmatic metal deposits. Elements 13, 415–420.
Maier, W.D., Barnes, S.J., Marsh, J.S., 2003. The concentrations of the noble metals in Southern African flood-type basalts and MORB: implications for petrogenesis and magmatic sulphide exploration. Contrib. Mineral. Petrol. 146, 44–61.
Maier, W.D., Barnes, S.J., Groves, D.I., 2013. The Bushveld complex, South Africa: formation of platinum-palladium, chrome- and vanadium-rich layers via hydrodynamic sorting of a mobilized cumulate slurry in a large relatively slowly cooling, subsiding magma chamber. Mineralium Deopsita 48, 1–56.
Maier, W.D., Howard, H.M., Smithies, R.H., Yang, S.H., Barnes, S.J., O'Brien, H., Huhma, H., Gardoll, S., 2015. Magmatic ore deposits in mafic–ultramafic intrusions of the Giles Event, Western Australia. Ore Geol. Rev. 71, 405–436.
Maier, W.D., Barnes, S.J., Karykowski, B.T., 2016. A chilled margin of komatiite and Mg-rich basaltic andesite in the western Bushveld complex, South Africa. Contrib. Mineral. Petrol. 171, 1–22.
Maier, W.D., O'Brien, H., Peltonen, P., Barnes, S.J., 2017. Platinum-group element contents of Karelian kimberlites: Implications for the PGE budget of the sub-continental lithospheric mantle. Geochim. Cosmochim. Acta 216, 358–371.
Maier, W.D., Halkoaho, T., Huhma, H., Hanski, E., Barnes, S.J., 2018. The Penikat intrusion, Finland: geochemistry, geochronology, and origin of platinum- palladium reefs. J. Petrol. 59, 967–1006.
Mansur, E., Barnes, S.J., Janasi, V., Henrique-Pinto, R., Alves, A., Marteleto, N.S., 2021. The distribution of platinum-group elements and Te, as, Bi, Sb and Se (TABS+) in the Paraná Magmatic Province: Effects of crystal fractionation, sulfide segregation and magma degassing. Lithos 400–401, 106374.
McDonough, W.F., Sun, S.S., 1995. The composition of the Earth. Chem. Geol. 120, 223–253.
Meisel, T.C., 2016. Rhodium. In: White, W.M. (Ed.), Encyclopedia of Geochemistry, Encyclopedia of Earth Sciences Series. Springer, pp. 1314–1316.
Mikkola, P., Huhma, H., Heilimo, E., Whitehouse, M., 2011. Archean crustal evolution of the Suomussalmi district as part of the Kianta complex, Karelia: Constraints from geochemistry and isotopes of granitoids. Lithos 125, 287–307.
Mokrushin, A.V., Smol'kin, V.F., Garuti, G., 2021. Chromite mineralization in the Sopcheozero deposit (Monchegorsk layered intrusion, Fennoscandian Shield). Minerals 11, 772.
Müller, W., Shelley, M., Miller, P., Broude, S., 2009. Initial performance metrics of a new custom-designed ArF excimer LA-ICPMS system coupled to a two-volume laser-ablation cell. J. Anal. At. Spectrom. 24, 209–214.
Mutanen, T., 1997. Geology and ore petrology of the Akanvaara and Koitelainen mafic layered intrusions and the Keivitsa-Satovaara layered complex, northern Finland. Geol. Survey Finland, Bulletin 395.
Naldrett, A.J., 2004. Magmatic Sulfide Deposits. Springer, Heidelberg, p. 728.
Park, J.W., Campbell, I.H., Arculus, R.J., 2013. Platinum-alloy and sulfur saturation in an arc-related basalt to rhyolite suite: evidence from the Pual Ridge lavas, the Eastern Manus Basin. Geochim. Cosmochim. Acta 101, 76–95.
Pearson, D.G., Canil, D., Shirey, S.B., 2003. Mantle samples included in volcanic rocks: xenoliths and diamonds. In: Treatise on Geochemistry. The Mantle, Vol. 2. Elsevier, New York, pp. 171–275.
Peltonen, P., Brügmann, G., 2006. Origin of layered continental mantle (Karelian craton, Finland): Geochemical and Re-Os isotope constraints. Lithos 89, 405–423.
Puchtel, I.S., Hofmann, A.W., Mezger, K., Shchipansky, A.A., Kulikov, V.S., Kulikova, V., 1996. Petrology of a 2.41 Ga remarkably fresh komatiitic basalt lava lake in Lion Hills, central Vetreny Belt, Baltic Shield. Contrib. Mineral. Petrol. 124, 273–290.

Puchtel, I.S., Haase, K.M., Hofmann, A.W., Chauvel, C., Kulikov, V.S., Garbe-Schönberg, C.D., Nemchin, A.A., 1997. Petrology and geochemistry of crustally contaminated komatiitic basalts from the Vetreny Belt, southeastern Baltic Shield: Evidence for an early Proterozoic mantle plume beneath rifted Archean continental lithosphere. Geochim. Cosmochim. Acta 61, 1205–1222.

Puchtel, I.S., Hofmann, A.W., Mezger, K., Jochum, K.P., Shchipansky, A.A., Samsonov, A., 1998. Oceanic plateau model for continental crustal growth in the Archaean: a case study from the Kostomuksha greenstone belt, NW Baltic Shield. Earth Planet. Sci. Lett. 155, 57–74.

Rankenburg, K., Lassiter, J.C., Brey, G., 2004. Origin of megacrysts in volcanic rocks of the Cameroon volcanic chain - Constraints on magma genesis and crustal contamination. Contrib. Mineral. Petrol. 147, 129–144.

Rivas, I., 2022. Faculty of Technology Sr Isotope Stratigraphy across the Paasivaara PGE Reef of the Penikat Intrusion, Northern Finland: Insights into the Genesis of Reef-Type PGE Mineralization. Master dissertation. University of Oulu.

Savard, D., Barnes, S.J., Meisel, T., 2010. Comparison between nickel-sulfur fire assay te co-precipitation and isotope dilution with high-pressure asher acid digestion for the determination of platinum-group elements, rhenium and gold. Geostand. Geoanal. Res. 34, 281–291.

Schissel, D., Tsvetkov, A.A., Mitrofanov, F.P., Korchagin, A.U., 2002. Basal platinum-group element mineralization in the Federov Pansky Layered mafic intrusion, Kola Peninsula, Russia. Econ. Geol. 97, 1657–1677.

Sharpe, M.R., Bahat, D., von Gruenewaldt, G., 1981. The concentric elliptical structure of feeder sites to the Bushveld complex and possible economic implications. Trans. Geol. Soc. S. Afr. 84, 239–244.

Shimizu, K., Nakamura, E., Maruyama, S., 2005. The geochemistry of ultramafic to mafic volcanics from the Belingwe greenstone belt, Zimbabwe: Magmatism in an Archean continental large igneous province. J. Petrol. 46, 2367–2394.

Shirey, S.B., Walker, R.J., 2003. The Re-Os isotope system in cosmochemistry and high-temperature geochemistry. Annu. Rev. Earth Planet. Sci. 26, 423–500.

Smith, W.D., Maier, W.D., 2021. The geotectonic setting, age and mineral deposit inventory of global layered intrusions. Earth Sci. Rev. 220, 103736.

Sobolev, A.V., Hofmann, A.W., Kuzmin, D.V., Yaxley, G.M., Arndt, N.T., Chung, S.L., Danyushevsky, L.V., Elliott, T., Frey, F.A., Garcia, M.O., Gurenko, A.A., Kamenetsky, V.S., Kerr, A.C., Krivolutskaya, N.A., Matvienkov, V.V., Nikogosian, I. K., Rocholl, A., Sigurdsson, I.A., Sushchevskaya, N.M., Teklay, M., 2009. The amount of recycled crust in sources of mantle-derived melts. Science 324, 89–91.

Sobolev, A.V., Asafov, E.V., Gurenko, A.A., Arndt, N.T., Batanova, V.G., Portnyagin, M. V., Garbe-Schönberg, D., Wilson, A.H., Byerly, G.R., 2019. Deep hydrous mantle reservoir provides evidence for crustal recycling before 3.3 billion years ago. Nature 571, 555–559.

Sun, S.-S., McDonough, W.F., 1989. Chemical and isotopic systematics of oceanic basalts: implications for mantle composition and processes. Geol. Soc. Lond., Spec. Publ. 1989, 313–345.

Vogel, D.C., Vuollo, J.I., Alapieti, T.T., James, R.S., 1998. Tectonic, stratigraphic, and geochemical comparisons between ca. 2500-2440 Ma mafic igneous events in the Canadian and Fennoscandian Shields. Precambrian Res. 92, 89–116.

Vuollo, J., Huhma, H., 2005. Paleoproterozoic mafic dikes in NE Finland. In: Lehtinen, M., Nurmi, P., Rämö, O.T. (Eds.), Precambrian Bedrock of Finland – Key to the Evolution of the Fennoscandian Shield, pp. 195–236.

Wang, C.Y., Zhou, M.F., Qi, L., 2007. Permian flood basalts and mafic intrusions in the Jinping (SW China)-Song Da (northern Vietnam) district: Mantle sources, crustal contamination and sulfide segregation. Chem. Geol. 243, 317–343.

Wang, C.Y., Zhou, M.-F., Qi, L., 2011. Chalcophile element geochemistry and petrogenesis of high-Ti and low-Ti magmas in the Permian Emeishan large igneous province, SW China. Contrib. Mineral. Petrol. 161, 237–254.

Yang, S.H., Maier, W.D., Lahaye, Y., O'Brien, H., 2013. Strontium isotope disequilibrium of plagioclase in the Upper critical Zone of the Bushveld complex: evidence for mixing of crystal slurries. Contrib. Mineral. Petrol. 166, 959–974.

Yang, S.H., Hanski, E., Li, C., Maier, W.D., Huhma, H., Mokrushin, A., Latypov, R., Lahaye, Y., O'Brien, H., Qu, W.J., 2016. Mantle source of the 2.44–2.50 Ga mantle plume-related magmatism in the Fennoscandian Shield: evidence from Os, Nd, and Sr isotope compositions of the Monchepluton and Kemi intrusions. Mineralium Deopsita 51, 1055–1073.

Yang, S.H., Maier, W.D., Godel, B., Barnes, S.J., Hanski, E., O'Brien, H., 2019. Parental magma composition of the Main Zone of the Bushveld complex: evidence from in situ LA-ICP-MS trace element analysis of silicate minerals in the cumulate Rocks. J. Petrol. 60, 359–392.